

Xray-Visual Models: Scaling Vision models on Industry Scale Data

Shlok Mishra¹, Tsung-Yu Lin¹, Linda Wang¹, Hongli Xu¹, Yimin Liu¹, Michael Hsu¹, Chaitanya Ahuja¹, Hao Yuan¹, Jianpeng Cheng¹, Hong-You Chen¹, Haoyuan Xu¹, Chao Li^{1,2}, Abhijeet Awasthi¹, Jihye Moon¹, Don Husa¹, Michael Ge¹, Sumedha Singla¹, Arkabandhu Chowdhury¹, Phong Dingh¹, Satya Narayan Shukla¹, Yonghuan Yang¹, David Jacobs^{1,3}, Qi Guo¹, Jun Xiao¹, Xiangjun Fan¹, Aashu Singh¹

¹Meta-AI, ²MIT (work done while at Meta AI), ³University of Maryland (work done while at Meta AI)

We present Xray-Visual, a unified vision model architecture for large-scale image and video understanding trained on industry-scale social media data. Our model leverages over 15 billion curated image-text pairs and 10 billion video-hashtag pairs from Facebook and Instagram, employing robust data curation pipelines that incorporate balancing and noise suppression strategies to maximize semantic diversity while minimizing label noise. We introduce a three-stage training pipeline that combines self-supervised MAE, semi-supervised hashtag classification, and CLIP-style contrastive learning to jointly optimize image and video modalities. Our architecture builds on a Vision Transformer backbone enhanced with efficient token reorganization (EViT) for improved computational efficiency. Extensive experiments demonstrate that Xray-Visual achieves state-of-the-art performance across diverse benchmarks, including ImageNet for image classification, Kinetics and HMDB51 for video understanding, and MSCOCO for cross-modal retrieval. The model exhibits strong robustness to domain shift and adversarial perturbations. We further demonstrate that integrating large language models as text encoders (LLM2CLIP) significantly enhances retrieval performance and generalization capabilities, particularly in real-world environments. Xray-Visual establishes new benchmarks for scalable, multimodal vision models, while maintaining superior accuracy and computational efficiency.

Date: February 20, 2026

Correspondence: shlok.mishra@meta.com



1 Introduction

Recent years have witnessed extraordinary advances in computer vision, particularly in image and video understanding, driven by innovations in deep learning architectures and large-scale pre-training objectives (He et al., 2015; Chen et al., 2020; He et al., 2020; Radford et al., 2021b; Mu et al., 2021; Zhai et al., 2023b; Kay et al., 2017). Despite these achievements, vision models still lag behind large language models (LLMs) in terms of data scale and generalization (Touvron et al., 2023b; Brown et al., 2020; Brown, 2020). The success of LLMs is largely attributed to the abundance of human-generated text available for training, whereas visual data at comparable scale remains challenging to collect and curate. This disparity has limited the progress of vision pre-training, especially in achieving robust performance across diverse, real-world scenarios.

To address this gap, we introduce a new family of unified vision models trained on billions of social media images and videos, setting new state-of-the-art (SOTA) results on both academic benchmarks and real-world tasks. Our approach is grounded in a comprehensive data curation pipeline that transforms raw, noisy corpora—initially exceeding 100 billion images and videos—into high-quality, semantically rich supervision. The ViSE image dataset comprises of over 10 billion image-text pairs sourced from public Facebook and Instagram posts, with captions and hashtags meticulously cleaned, filtered for English, and balanced to ensure broad semantic coverage. For video understanding, we curate 10 billion video-hashtag pairs from 24 billion Instagram posts, employing canonicalization and long-tail resampling to guarantee adequate representation of rare visual concepts. In Fig 2 we show that we train on 26 Billion images and videos which is the largest

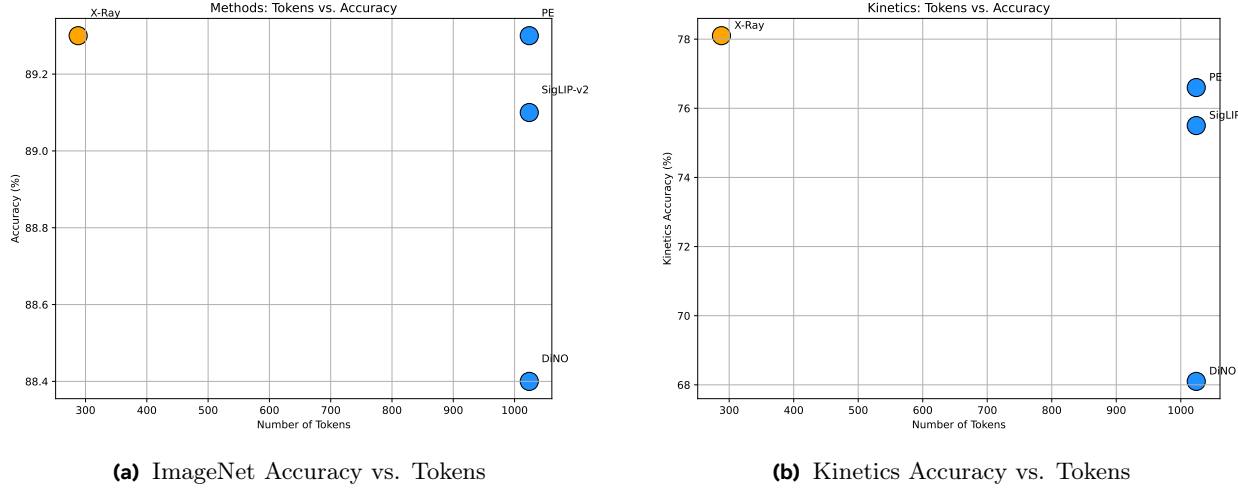
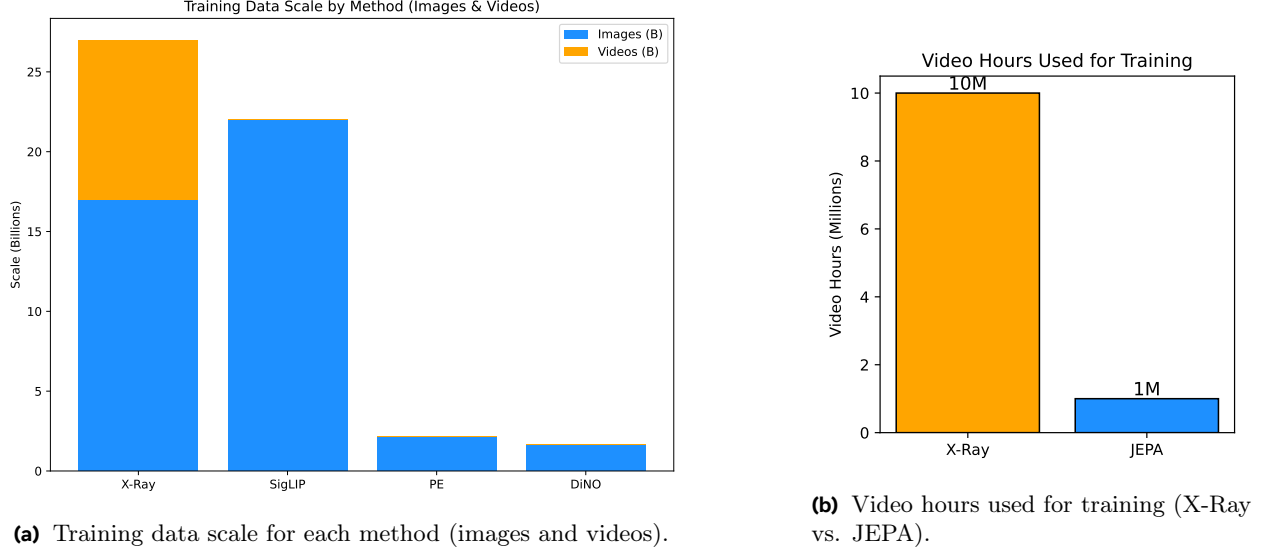


Figure 1 XRay achieves 89.3% Top-1 accuracy with 336px and 288 tokens, vs. baselines at 448px/1024 tokens. This is a 71.9% token reduction, 43.75% pixel area reduction, and 84.2% reduction in the product proxy (6.3 \times lower combined cost).

amount of pre-training in publically available vision encoder pre-training. For videos we train on 10 billion videos which is close to 10m hours of video data, which is 10x more than world models like JEPA [Assran et al. \(2025\)](#) as shown in Fig 2b. Supervision quality is further enhanced by generating synthetic captions for both images and videos using [Grattafiori et al. \(2024\)](#), followed by text only LLM-based rewriting [Fan et al. \(2023b\)](#) to increase diversity and reduce repetition ([Touvron et al., 2023b](#)).

Our models employ a unified architecture that jointly processes images and videos, enabling robust multimodal representation learning. This is done by extending the Vision Transformer (ViT) backbone ([Dosovitskiy et al., 2021](#)) with 3D tokenization [Tran et al. \(2015\)](#), allowing seamless handling of multiple modalities within a single framework. Our primary vision backbone follows EViT [Liang et al. \(2022\)](#); which focuses on efficiency while maintaining high performance. EViT ([Liang et al., 2022](#)), reorganizes and drop inattentive tokens, supporting higher input resolutions with minimal computational overhead. Register tokens are appended to the transformer sequence ([Dariset et al., 2023](#)), enhancing the model’s ability to capture outlier features and boosting video performance. The training pipeline consists of three key stages: (1) self-supervised masked autoencoding (MAE) ([He et al., 2022](#)) for learning visual representations from masked patches in images and videos; (2) semi-supervised hashtag classification leveraging large-scale hashtag-labeled datasets; and (3) CLIP-style contrastive learning ([Radford et al., 2021b](#)) using curated image and video caption pairs to align visual and textual representations. Additional objectives such as denoising ([Chen et al., 2024](#)) and SLIP (Self-supervision meets Language-Image Pre-training) ([Mu et al., 2021](#)) further strengthen the learned features. Notably, we replace standard text encoders with LLaMA-1b ([Touvron et al., 2023b](#)), which proves critical for high-performance retrieval on real world datasets and internal metrics.

Empirically, our pure image models achieve SOTA 89.3% accuracy on ImageNet [Deng et al. \(2009\)](#), while the unified image-video architecture attains 88.1% on ImageNet and 78.1% on Kinetics — accomplished with lower (336)input resolutions and only 1/4th (288 tokens) the tokens compared to other leading vision models like PE [Bolya et al. \(2025\)](#), SigLIP ([Tschanne et al., 2025](#); [Zhai et al., 2023b](#)), which use 448 resolution and 1024 tokens as can be seen in Fig 1a and Fig 1b. We also observe that our joint image-video model trained on both image and video is better for video understanding then pure video only models; due to the synergy of image and video and cross domain information. It’s also almost SOTA on image bechmarks and achieves 88.1% only 1.2% below pure image models. We also set new SOTA benchmarks on MS-COCO [Chen et al. \(2015\)](#) image-to-text and text-to-image retrieval. Across a wide range of data scales, our models demonstrate strong generalization and robust out-of-distribution (OOD) performance. Most importantly, we show that existing vision encoders suffer significant performance drops on real-world data distributions, whereas our LLM text encoder based models consistently deliver best-in-class results on complex, production-scale retrieval tasks.



(a) Training data scale for each method (images and videos).

(b) Video hours used for training (X-Ray vs. JEPA).

Figure 2 Comparison of training data scale across vision models. (a) XrayVisual leverages the largest curated dataset for vision encoder training to date, (b) We utilize 10 \times more video data than state-of-the-art world models such as V-JEPA [Assran et al. \(2025\)](#).

Overview of Contributions Our main contributions are summarized below.

• **Data collection**

- We show a systematic study of how to train vision models on industry scale data. We developed a comprehensive data curation pipeline for large-scale vision model training, starting from over 100 billion raw social media images and videos.
- We curate two large-scale datasets: (1) ViSE image dataset with over 15 billion image-text pairs from public Facebook and Instagram posts, applying rigorous cleaning (removal of URLs, emojis, user tags, and non-semantic content), language detection for English captions, and WordNet synset-based resampling to balance semantic diversity across the long-tail distribution, and (2) a video dataset with 10 billion video-hashtag pairs from 24 billion Instagram posts, with canonicalized hashtags and resampling to ensure robust representation of both common and rare visual concepts.

• **Model Architecture and Training**

- We proposed a unified model architecture that begins with self-supervised masked autoencoding (MAE) for initial representation learning, followed by fine-tuning with hashtag classification, and culminating in CLIP-style contrastive training using curated image and video caption pairs.
- Incorporated denoising loss and added LLM’s as the text encoder during training to further enhance scaling behavior and robustness, demonstrating that larger models and datasets yield consistent performance improvements and LLM’s help in real world generalization.
- Designed a joint image-video architecture based on Vision Transformers, enabling simultaneous learning from both modalities. This joint approach significantly improves video representations and remains highly competitive for image tasks, eliminating the need for separate models.

• **Efficiency and Performance**

- We achieved state-of-the-art results on major benchmarks including ImageNet, Kinetics, MS-COCO, and various out-of-distribution (OOD) datasets, validating the model’s generalization and robustness.
- Demonstrated that our model operates at a 336 input resolution while utilizing only 25% of the tokens (288 tokens) compared to Perception Encoder (PE) [Bolya et al. \(2025\)](#), DiNO (1024 tokens)

Siméoni et al. (2025), SigLIP Tschannen et al. (2025) resulting in a 4x increase in queries per second (QPS) and substantial computational efficiency.

- Due to training on large scale datasets, Despite the reduced token usage and higher efficiency, our model consistently outperforms or matches the best existing models on both academic and real-world tasks.

2 Data

In this section we discuss the details of data curation. Our training pipeline is in three stages, we begin with MAE followed by finetuning and in third stage we use CLIP training. We use different datasets in different stages. We begin with describing image data for all the three stages followed by details of video data.

2.1 Image Dataset - ViSE

We assembled a large-scale, high-quality dataset of image-text pairs from Facebook and Instagram called ViSE. Raw social media captions typically contain extraneous content such as URLs, email addresses, emojis, user tags, and non-semantic characters. We applied rigorous post-processing to remove these elements and retain only meaningful text, including removing the pound sign from hashtags while preserving the hashtag text.

Semantic balancing A key challenge in web-scale data curation is the imbalanced distribution of visual concepts Radford et al. (2021a). We leveraged WordNet synsets to identify visually relevant concepts and deduplicate synonyms. To address the long-tail distribution, we resampled the dataset by undersampling frequent (head) concepts and oversampling rare (tail) concepts. Specifically, we segmented captions into sentences using a custom UDF, associating each image with multiple sentences as distinct pairs. We computed unigram frequencies (excluding English stopwords) and resampled accordingly. As shown in Table 1, this balancing strategy yielded a 7.3% improvement in ImageNet linear probe accuracy for ViT-B models trained from scratch for 700K iterations.

Method	Accuracy
ViSE without resampling	65.4%
ViSE with resampling	72.7%

Table 1 Impact of semantic resampling on ImageNet linear classification accuracy.

Noise suppression To mitigate noise inherent in web-scale data, we applied similarity-based filtering using a pre-trained MetaCLIP Xu et al. (2023) model to score image-text alignment. We experimented with various similarity thresholds and additionally incorporated label smoothing into the contrastive loss. Table 2 shows that filtering with a 0.25 similarity threshold combined with label smoothing achieved the best results, improving ImageNet linear classification accuracy from 71.7% to 72.8%. All models were trained for 200K iterations. The final ViSE dataset contains approximately 10 billion high-quality image-text pairs, making it one of the largest datasets used for CLIP-style training Schuhmann et al. (2022); Xu et al. (2023); Chuang et al. (2025).

Filtering	Method	Top-1 Accuracy (%)
	Resampling	71.7
✓	+ Filtering	72.8

Table 2 Ablation study on ImageNet linear classification: impact of similarity-based filtering.

2.2 Video Data

To train high-quality multimodal representations, we curate a large-scale video-text dataset from Instagram posts called URU. Unlike user-provided captions for videos, which are often generic or noisy, hashtags typically contain more precise visual and semantic descriptors directly relevant to video content. We systematically process hashtags from billions of public Instagram posts containing videos, resulting in a curated collection of ~ 5 billion video-hashtag pairs.

Hashtag Processing and Canonicalization User-provided hashtags can be inherently noisy and irrelevant. To improve data quality and hashtag effectiveness, we follow the procedure of prior work [Singh et al. \(2022\)](#) for images with additional optimizations to extract meaningful hashtags for training purposes. We leveraged WordNet synsets to identify hashtags related to meaningful objects. We then map semantically similar hashtags to canonical representations, creating ~ 75 k user-provided hashtag - canonical hashtag pairs. This canonicalization process reduces vocabulary size while improving semantic consistency and training stability.

Video-Hashtag Pair Construction When any user-provided hashtag can be mapped to our user-provided - canonical hashtag pairs, videos - user-provided hashtag pair is retrieved to construct a new video - canonical hashtag pair. After addressing the long-tail distribution by downsampling frequent hashtags and oversampling rare hashtags, we generated ~ 5 billion video - canonical hashtags pairs.

Adapted Data for Training Strategy As described in Section 4.2, we adopt a three-stage pre-training process. To adapt our training strategy, we utilized different types of hashtags as supervisory signals, following the findings in [Ghadiyaram et al. \(2019\)](#). Importantly, our larger scale datasets are designed to promote general visual understanding capabilities, rather than overlapping with target datasets such as IG-Kinetics described in the same study. For the first-stage self-supervised MAE and the second-stage semi-supervised hashtag classification, we employed URU-Video-Noun-5B, which focuses exclusively on hashtags related to visual objects. To further enhance the model’s capacity for action understanding alongside object recognition, we expanded the hashtag set and construct URU-Video-Action-5B for the third-stage CLIP training.

Dataset	Total #labels(hashtags)
IG-Kinetics	359
URU-Video-Noun-5B	22013
URU-Video-Action-5B	31619

Table 3 Comparison of label scale across video-hashtag datasets. IG-Kinetics [Ghadiyaram et al. \(2019\)](#) uses 400 action labels from Kinetics as seed labels, resulting in 359 unique labels. In contrast, the URU-Video datasets leverage a broader vocabulary filtered from WordNet synsets, yielding significantly more labels and supporting richer visual and action concept coverage.

2.3 Synthetic Captions

Synthetic data generation has become an effective strategy for training vision-language models [Fan et al. \(2023a\)](#); [Zhu et al. \(2025\)](#); [Team et al. \(2024\)](#); [Touvron et al. \(2023b\)](#). We generated synthetic captions using an internal multimodal large language model (MMLM) trained on Facebook and Instagram videos and reels.

Our experiments revealed a trade-off: while synthetic captions significantly improved retrieval performance compared to user-generated captions, they led to decreased video classification accuracy. We hypothesized that this degradation stemmed from quality issues in the generated captions, particularly repetitive phrasing. Analysis revealed approximately 3% repetition our video captions. To fix this we propose to use LLM based rewrites which we mention in next section.

2.3.1 LLM-Based Caption Refinement

To address caption quality issues, we leveraged LLM-based rewriting [Fan et al. \(2023a\)](#), which has been shown to increase diversity in sentence structure and vocabulary while preserving semantic content. We employed Llama 3B [Grattafiori et al. \(2024\)](#) to refine the synthetic captions, using prompts such as “rewrite this caption

of a video vividly, and keep it less than thirty words.” This approach effectively eliminated repetitive elements and produced more concise, descriptive captions.

2.4 Other datasets

We also use MetaCLIP [Chuang et al. \(2025\)](#) dataset for pre-training. MetaCLIP dataset is very helpful specially for pre-training for captioning realted tasks. Whenver we are pre-training for MMLM’s we found that higher quality metaclip dataset had higher performance for downstream captioning tasks. However in general for internal embedding related tasks using MetaCLIP we saw regresstion on internal retrieval tasks. We also hashtag the dataset for images (~ 5 B images) and videos (~ 5 B videos) for second-stage pre-training expanding [Mahajan et al. \(2018\)](#).

3 Model architecture

Generally, computer vision models employ distinct architectures for image and video tasks ([Chen et al., 2020](#); [Caron et al., 2021](#); [He et al., 2022](#)). However, for large-scale industrial training, it is desirable to leverage both image and video datasets jointly to obtain richer representations. To this end, we adopt a co-training approach, training on both images and videos simultaneously. We observe that joint training consistently improves video performance while maintaining strong image performance. An additional benefit of a unified architecture is the reduced deployment overhead, as a single model can be used for both modalities, eliminating the need to maintain and deploy separate models for images and videos.

3.1 Design Architecture

The base backbone used in XrayVisual training is the Vision Transformer (ViT) architecture [Dosovitskiy et al. \(2021\)](#). To enable joint training on both images and videos, we conducted extensive ablation studies and selected a video ViT backbone with 3D tokenization for XrayVisual. Special consideration is required when processing image inputs. Specifically, we repeat each image along the temporal dimension to match the kernel size of the 3D convolution, and apply zero-padding and unpadding to accommodate the positional embeddings. For video inputs, no such modification is necessary: the 3D convolution operates directly on the full video sequence without the need for zero-padding.

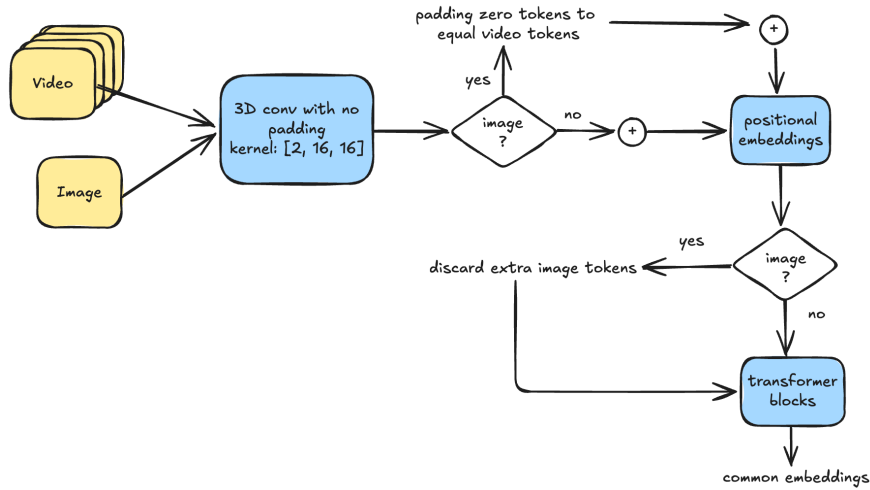


Figure 3 XRV Architecture: XrayVisual uses a Vision Transformer (ViT) [Dosovitskiy et al. \(2021\)](#) backbone with 3D tokenization for joint image-video training. Images are repeated along the temporal dimension with zero-padding to match the 3D convolution kernel and positional embeddings, while videos are processed directly without modification.

3.2 EViT-2b

For optimal performance, we employ larger 2 billion parameter models utilizing the EViT architecture [Liang et al. \(2022\)](#).

Efficient high-resolution processing While higher input resolutions capture more detailed visual information and typically improve recognition accuracy [Dosovitskiy et al. \(2021\)](#), they pose computational challenges for vision transformers. Specifically, increasing input resolution leads to quadratic growth in the number of tokens, substantially increasing computational cost. To mitigate this issue, we adopt the token reorganization technique from EViT [Liang et al. \(2022\)](#), which selectively prunes inattentive tokens to improve efficiency while preserving accuracy.

The EViT method computes attention weights from the CLS token to all patch tokens, identifying those with low attention scores as inattentive. By tuning the keep rate hyperparameter, we can achieve a favorable trade-off between computational efficiency and task performance. Empirically, we find that removing inattentive tokens incurs only negligible accuracy degradation while enabling the model to process higher-resolution inputs and achieve superior overall performance.

We adapt this technique to image-text contrastive learning and observe approximately 0.5% improvement over standard ViT models. Following the EViT protocol [Liang et al. \(2022\)](#), we uniformly select three transformer layers for token reorganization. Table 4 presents our results, where throughput (images/sec) is measured on a single V100 GPU. Based on these experiments, we adopt 288×288 resolution for ViT-B16 and 336×336 resolution for models larger than ViT-H14. All final results are reported using a 2 billion parameter model with EViT.

Model	Resolution	Keep Rate	Throughput	LC (%)	ZS (%)
ViT-B16	224	1.0	227.23	83.11	72.24
ViT-B16	288	0.7	281.87	83.57	72.79
ViT-B16	336	0.5	219.25	83.27	72.55
ViT-H14	224	1.0	29.85	86.99	79.05
ViT-H14	280	0.7	25.90	86.77	79.11
ViT-H14	336	0.5	23.87	87.38	80.03

Table 4 Model Performance at Different Resolutions and Keep Rates.

4 Training

In this section we describe our training methodology beginning with batch sampling Strategy, followed by our three stage training pipeline.

4.1 Multi-Modal Batch Sampling Strategy

We observe that the distribution of image and video data during joint training significantly impacts model performance. Prolonged consecutive exposure to a single modality can introduce bias toward that modality. Our experiments reveal that the critical factor is not the absolute quantity of data from each modality, but rather the frequency and uniformity with which the model encounters both modalities during training. While moderately imbalanced image-to-video ratios (up to 1:10) remain acceptable, it is essential to distribute batches from both modalities uniformly throughout each epoch, preventing extended periods of single-modality exposure.

In our training scheme, each batch contains data from only one modality. Through extensive experimentation, we identify the optimal strategy: sampling image or video batches according to a predefined probability that ensures both modalities are exhausted approximately simultaneously within each epoch. This approach uniformly distributes the smaller modality across the larger one, maintaining balanced exposure throughout training.

Formally, consider a scenario with N_I image samples (batch size B_I) and N_V video samples (batch size B_V). The sampling probabilities for image and video batches are computed as:

$$P_I : P_V = \frac{N_I}{B_I} : \frac{N_V}{B_V}$$

For example, with 5B image samples (batch size 64) and 2B video samples (batch size 32), the ratio becomes $(5/64) : (2/32) = 5 : 4 = 0.56 : 0.44$. Thus, at each iteration, the model samples an image batch with probability 0.56 and a video batch with probability 0.44.

Table 5 demonstrates the importance of selecting an appropriate batch sampling strategy, evaluated using ViT-L on URU training data with an image-to-video ratio of 5B:500M.

Batch Sampling Strategy	ImageNet LP	Kinetics Top-1
Strict alternation; new epoch starts after image modality finishes, resulting in image-only training after video modality exhaustion	86.03%	71.2%
Strict alternation; video modality repeats after exhaustion	80.56%	73.3%
Probabilistic sampling; both modalities finish epoch simultaneously (Ours)	84.16%	74.1%

Table 5 Comparison of batch sampling strategies on ImageNet linear probing accuracy and Kinetics Top-1 accuracy.

4.2 Multi-Stage Training Strategy

Our training strategy consists of a three-stage pre-training process: (1) self-supervised learning via Masked Autoencoding (MAE) [He et al. \(2022\)](#), (2) semi-supervised hashtag classification, and (3) semi-supervised contrastive learning with image/video-caption pairs. Figure 4 illustrates this progressive training pipeline.

The first two stages follow the MAE pre-pre-training framework described in [Singh et al. \(2023\)](#). Prior work has demonstrated that MAE pre-training exhibits favorable scaling properties with respect to both dataset and model size, and that combining MAE with weak supervision further enhances large-scale vision models [Singh et al. \(2023\)](#). This combination not only accelerates convergence but also provides a simple and scalable approach for learning visual representations at scale.

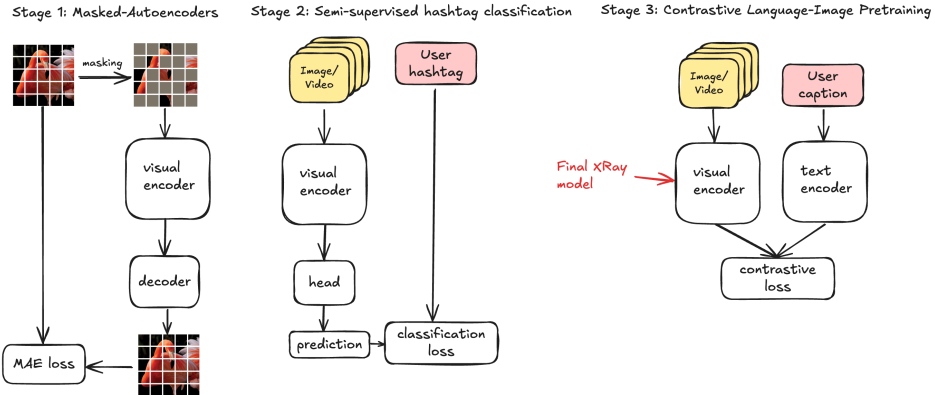


Figure 4 Our three-stage training pipeline consists of MAE pre-training, followed by hashtag classification, and followed by CLIP-style contrastive learning.

4.2.1 Stage 1: Masked Autoencoding

MAE [He et al. \(2022\)](#) learns visual representations from unlabeled image and video datasets through reconstruction. We adopt MAE as our initial stage due to its strong scaling behavior with respect to both

model and dataset size. The MAE framework randomly masks 75% of image patches and trains the model to reconstruct the masked input by minimizing pixel reconstruction error. For videos, we apply a higher masking ratio of 90% following [Feichtenhofer et al. \(2022\)](#). The target pixel values for each patch are normalized by the patch-wise mean and standard deviation.

Leveraging the ViT architecture, MAE training operates on only the 25% unmasked patches, while a separate lightweight decoder reconstructs the missing regions. This asymmetric encoder-decoder design enables highly efficient training and supports the use of larger visual encoders.

4.2.2 Stage 2: Semi-Supervised Hashtag Classification

Following MAE pre-training, we employ hashtag classification. We find this semi-supervised approach highly effective, yielding results comparable to training on dedicated video and image baselines respectively. The data for both the first and second stages is sourced from the URU nouns hashtags dataset, enabling the model to learn robust object-centric representations. We can see in Table 6 row-1 that our hashtag finetuned model is pretty strong and gives very solid Kinetics and ImageNet performance.

4.2.3 Stage 3: Contrastive Learning with Captions

In the final stage, we introduce CLIP-style training [Radford et al. \(2021a\)](#) using image and video caption data. CLIP is well-established for its strong generalization capabilities in computer vision and exhibits excellent scaling behavior, which we corroborate in our internal experiments. For this stage, we leverage ViSE data curated from user captions for images, and URU actions data for videos, as the latter emphasizes action understanding. Notably, the data used in the first two stages primarily focuses on noun-centric visual concepts, while the third stage emphasizes verb-centric action understanding, enabling the model to learn comprehensive representations encompassing both objects and actions. We can see in Table 6 row-2 has very strong zero shot generalization due to clip training and strong linear probing.

Table 6 presents ablation results for different pre-training strategies using the ViT-H backbone, demonstrating the progressive improvements from each stage and additional techniques.

Training Configuration	Spatial Size	K700 Top-1	IN Top-1
MAE → URU	280	75.1	87.1
MAE → URU → CLIP	280	75.2	87.3
+ Registers	280	75.4	87.3
+ Augmentations	280	76.1	87.6
+ SLIP	280	76.7	87.8

Table 6 Ablation study on training stages and techniques using ViT-H. K700: Kinetics-700, IN: ImageNet.

4.2.4 SLIP: Combining Self-Supervised and Supervised Learning

In addition to CLIP, we experiment with SLIP [Mu et al. \(2021\)](#), which integrates self-supervised and contrastive learning objectives. We utilize SimCLR [Chen et al. \(2020\)](#), a self-supervised contrastive learning method that has demonstrated significant progress in computer vision, often matching or surpassing supervised learning in tasks such as image recognition, object detection, and semantic segmentation [Caron et al. \(2021\)](#); [Chen et al. \(2020\)](#). Self-supervised image features have proven highly effective for grounding vision-language models (VLMs) and multimodal large language models (MM-LLMs) [Tong et al. \(2024\)](#), and are widely adopted for their generalization capabilities and robustness.

We employ SimCLR as our primary self-supervised learning module due to its demonstrated scalability on large-scale datasets such as JFT [Mishra et al. \(2022\)](#). SimCLR applies stochastic data augmentations—including random cropping, color distortions, and Gaussian blur—to generate pairs of correlated views from the same image, which serve as positive pairs. These augmented images are processed through a base encoder (typically a CNN or ViT), followed by a projection head that maps representations to a lower-dimensional space where

contrastive loss is applied. The projection head, implemented as a small multi-layer perceptron, facilitates the learning of discriminative features.

The contrastive loss maximizes agreement between embeddings of positive pairs while minimizing similarity to negative pairs (embeddings from different images). This objective encourages the model to learn invariant and robust features without relying on labeled data, significantly improving representation quality.

While standard SimCLR uses two random crops of the same image as positive samples, we extend this approach for video data to better capture temporal information: we sample two frames from the same video and treat them as positive pairs, enabling the model to learn temporally invariant video representations.

4.2.5 Denoising loss

In addition to the CLIP loss, we incorporate a denoising loss \mathcal{L}_{den} into our training objective. The denoising loss serves two primary purposes: (1) it stabilizes the training process and encourages the model to learn more robust visual representations and (2) it enhances scalability with respect to the number of training examples. This approach is motivated by prior work, which demonstrates the effectiveness of denoising objectives in large-scale vision models [Chen et al. \(2024\)](#). While [Chen et al. \(2024\)](#) focuses on deconstructing diffusion models into denoising networks for self-supervised learning on image data, our approach expands the applicability of the denoising loss in two significant ways. First, we directly inject noise to the XrayVisual output. This is unlike [Chen et al. \(2024\)](#), which adds noise to the PCA embedding space. This is crucial because the embedding space of the visual encoder is continually updated during training, which in turn modifies the eigenvector space. As the objective of the denoising encoder-decoder keeps getting moved with every iteration, it results in a less than optimal optimization. We validate this with subpar ImageNet accuracies on an ablation with a PCA bottleneck. By avoiding PCA, we ensure that the denoising process remains consistent and robust throughout training, regardless of changes in the encoder’s representation space. Second, we create an effective information bottleneck first down-projecting the XrayVisual embedding to 0.1x the size using an MLP encoder. We then add zero-mean random gaussian noise to the down-projected embedding followed by up-projecting MLPs as a decoder to reconstruct denoised embeddings. We use L2 norm as the reconstruction loss function which we denote as \mathcal{L}_{den} . This architecture allows us to learn a more flexible and expressive mapping for denoising, tailored to the evolving feature space of the visual encoder.

Robust Representations: Models trained with the denoising loss exhibit greater robustness to noise and perturbations in the input data. On a training run with 600k iterations, we observe that the ImageNet accuracy increases by 0.3% from 79.09% to 79.39% when the denoising loss is included.

Scalability: By adding the denoising loss, we also observe improved scalability as the number of training examples increase. This is particularly important for large-scale datasets, where contrastive losses may struggle to fully utilize the available data.

Our scaling experiments address the following research questions:

Scaling with Training Examples: Does the denoising loss improve model performance as the number of training examples increase?

The impact of the denoising loss is illustrated in Figure 5 which show overall improvement in ImageNet Accuracies as the number of unique examples in training data increase of 1B through 5B. Note that we run all models for the same number of iterations. Hence, in ablations with fewer training examples than number of iterations, we cycle through the same data again till we reach a total of 500k iterations.

Scaling with Model Size: Does the denoising loss have a similar scaling effect when applied to models of different sizes?

Importance of the Denoising Loss Scaling Parameter The scaling parameter for the denoising loss, denoted as λ_{den} is a critical hyperparameter in our setup. Through empirical analysis, we find that setting $\lambda_{den} = 1$ yields the best performance, providing a 0.3% accuracy gain over the XrayVisual model trained solely with the CLIP loss.

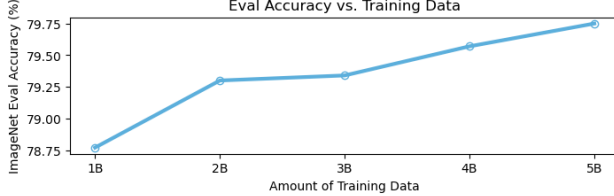


Figure 5 Scaling analysis. ImageNet zero-shot accuracy improves consistently as the number of unique training examples increases from 1B to 5B. EViT-2B models trained with denoising loss exhibit strong scaling behavior across all data regimes. All models are trained for 500K iterations.

4.3 Progressive resolution

Following the successful paradigm established by SiGLIP [Zhai et al. \(2023b,a\)](#) and Perception Encoder [Bolya et al. \(2025\)](#), we implement progressive resolution training during our CLIP model development. This multi-stage training approach enables efficient scaling while maintaining computational tractability across different resolution regimes. Our training curriculum consists of three distinct phases: the initial and secondary training stages operate at 224×224 resolution to establish foundational representations. The final training stage employs a progressive resolution schedule, systematically increasing input resolution through the sequence: $98 \times 98 \rightarrow 154 \times 154 \rightarrow 224 \times 224 \rightarrow 336 \times 336 \rightarrow 448 \times 448$. This graduated approach allows the model to adapt incrementally to higher-resolution inputs while leveraging previously learned features. We conducted comparative analysis with the FLIP (Fast Language-Image Pre-training) [Li et al. \(2022\)](#) methodology to evaluate alternative scaling strategies. Our empirical evaluation demonstrates that progressive resolution training achieves superior computational efficiency compared to the FLIP approach, while maintaining competitive performance across evaluation benchmarks. The progressive resolution strategy proves particularly advantageous for large-scale training scenarios, offering an optimal balance between computational cost and model capability development.

4.4 Registers

In the development of CLIP [Radford et al. \(2021a\)](#) and DINOv2 [Caron et al. \(2021\)](#), it was observed that certain tokens, referred to as outlier tokens, exhibit a norm approximately 10 times higher at the output and constitute a small fraction of the total sequence (around 2%). These tokens tend to emerge around the middle layers of the vision transformer and only become apparent after extensive training with sufficiently large transformers. Since XrayVisual involves large-scale CLIP training, we observed similar token behavior in XrayVisual. The introduction of registers in DINOv2, as detailed in [\(Dariset et al., 2023; Oquab et al., 2023\)](#), presents a significant advancement in handling image recognition tasks within large-scale training pipelines like XrayVisual. Registers are additional tokens appended to the token sequence of a vision transformer, independent of the input image. This modification addresses specific challenges observed in the DINOv2 model, particularly concerning the presence of these outlier tokens. After adding registers into our pipeline, we saw improvements in video understanding. We measured XrayVisual’s performance by evaluating image classification on ImageNet for image understanding and Kinetics-700 for video temporal understanding. On Kinetics-700, we observed a gain of 0.8% and a slight improvement (+0.3%) in image accuracy.

4.5 Lion optimizer

We adopt Lion [Chen et al. \(2023\)](#) as our optimizer, which was discovered through algorithmic program search. Prior work has demonstrated that Lion achieves a 2% improvement in ImageNet zero-shot accuracy for the BASIC model compared to Adafactor [Shazeer and Stern \(2018\)](#). To validate its effectiveness for our architecture, we conduct a direct comparison between Lion and AdamW optimizers. Following the recommendations in [Chen et al. \(2023\)](#), we configure Lion with momentum parameters $\beta_1 = 0.9$ and $\beta_2 = 0.99$. With this configuration, we observe a 0.3% improvement in ImageNet zero-shot accuracy when using Lion compared to AdamW, confirming the optimizer’s effectiveness for large-scale vision-language pre-training.

4.6 LLM as text encoder

We were currently using standard CLIP text encoder used for contrastive training. However it has has a couple limitations: Limited context window: can only process 77 tokens. Weak text comprehension: the text encoder is small and may not be able to understand the text describing the image/video. To solve this we initially tried scaling the text encoder and the finally we decided to use LLaMA-1b as our text encoder.

4.6.1 Scaling text encoder

The table below shows the improvement on ImageNet using larger text encoder in CLIP framework. We followed the setting presented in GPT-2 to increase the attention heads and transformer blocks. CLIP used a 12-layer-8-head base model as the text encoder. With increasing size, the model achieves better image-text alignment and hence higher zero-shot (ZS) accuracy while barely improves image encoder with marginal improvement on linear probing (LC) accuracy.

Heads	Layers	Embedding Dimension	LC (%)	ZS (%)
8	12	512	83.05	71.24
12	12	768	83.11	71.71
16	24	1024	83.11	71.91
20	36	1280	83.08	72.13

Table 7 Model Configuration and Performance

However we still didn't see improved performance with scaling text encoder; hence we started moving to LLM based CLIP models which we describe next.

4.6.2 LLaMA-1b text encoder

Large language models (LLMs) [Touvron et al. \(2023b\)](#); [Brown et al. \(2020\)](#); [Brown \(2020\)](#) demonstrate exceptional capabilities in processing extensive text corpora and handling long, complex sequences. Recent work in LLM2CLIP [Huang et al. \(2024\)](#) has shown that leveraging LLMs as text encoders yields significant improvements in retrieval performance. Building upon this foundation, we integrate LLMs as text encoders in our XRayVisual CLIP training to enhance retrieval capabilities. This approach offers additional advantages including support for long, dense captions and inherent multilingual capabilities.

LLM2CLIP Methodology. The LLM2CLIP framework consists of two primary components. Initially, the LLM undergoes fine-tuning using LoRA [Hu et al. \(2021\)](#) to achieve proper output space alignment. A critical observation from LLM2CLIP research reveals that vanilla LLM output features for different texts exhibit high similarity, resulting in insufficient discriminative power. This feature homogeneity severely impairs CLIP's contrastive learning objective, leading to suboptimal vision encoder performance when employing off-the-shelf LLMs.

Alignment and Fine-tuning Strategy. To address the discriminative power limitation, we adopt the LLM2Vec approach, which expands the LLM's attention mechanism to bidirectional processing and employs masked next token prediction for improved output space alignment of semantically similar texts. Subsequently, we perform caption contrastive fine-tuning using supervised SimCSE [Gao et al. \(2021\)](#) on MS-COCO [Chen et al. \(2015\)](#) captions and re-annotated captions generated by ShareCaptioner. This process optimizes the embedding space by bringing captions of identical images closer together while separating captions from different images.

Implementation Details. Our LLM2CLIP implementation utilizes LLaMA-1B [Touvron et al. \(2023b,a\)](#) as the text encoder backbone. During training, we fine-tune the CLIP vision encoder while maintaining the fine-tuned LLM in a frozen state. This freezing strategy provides dual benefits: reduced memory consumption critical for maintaining large batch sizes necessary for effective negative sampling, and preservation of the LLM's comprehensive open-world knowledge. To enhance alignment between the LLM and CLIP visual encoder, we incorporate an adapter module serving as learnable parameters. Following [Huang et al. \(2024\)](#), we implement a 4-layer adapter architecture. Projection layers are subsequently employed to ensure dimensional

compatibility between the two encoder modalities. Our training regimen incorporates both image-text and video-text pairs, with comprehensive experimentation across synthetic and user-generated caption datasets.

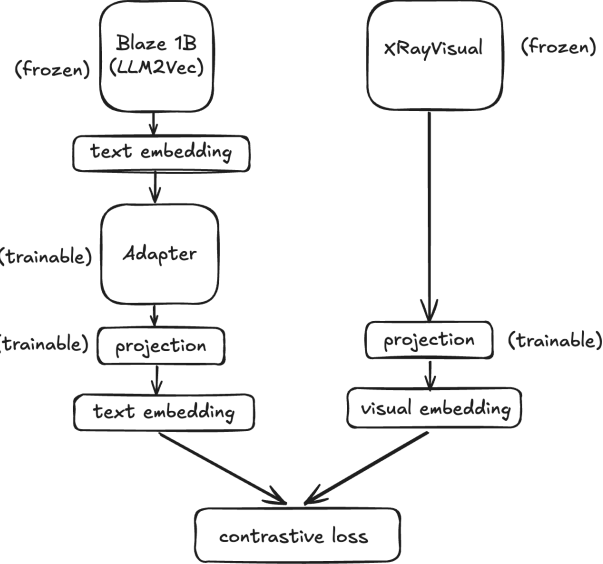


Figure 6 llm2clip

Table 8 Using LLM as text encoder zero-shot performance. Both of these models use ViT-H for vision encoder.

Models	COCO Img-Text r@1	COCO Text-Img r@1	MSRVTT Vid-Text r@1	MSRVTT Text-Vid r@1	ImageNet top-1	K700 top-1	Ads2Ads	IG Reels2Ads	FB Reels2Ads
XRay	48.21	31.12	51.4	27.92	79.19	61.53	88.27	62.42	70.76
LLM2CLIP	49.71	37.1	58.2	31.9	77.05	60.52	89.76	67.04	74.96

4.7 Efficiency with Token Merging

One of the primary objectives for deploying models at large scale is efficiency. To this end, we employ token merging to reduce computational overhead. We utilize ToMe (Token Merging) [Bolya et al. \(2022\)](#) to minimize the number of tokens processed in various layers of the ViT architecture, thereby reducing computation. This approach can be applied during both training and inference. Notably, we find that applying ToMe exclusively during inference results in minimal performance regression. Specifically, using ToMe with ViT-H at a spatial resolution of 280 during inference leads to less than a 0.5% drop in ImageNet accuracy and only a 0.04% drop on Kinetics, while video inference speed increases by 58%.

4.7.1 Synthetic Caption Generation and Refinement with Siamese loss

We utilize an internal multimodal large language model (MMLLM) to generate synthetic captions for videos. Despite the inherent noise in automatically generated captions, we observe substantial improvements, achieving a 6% gain on MSR-VTT media-to-text retrieval compared to using user-generated captions alone.

LLM-Based Caption Refinement Initial analysis revealed that a small fraction (less than 1%) of MMLLM-generated captions exhibited hallucinations, repetitive phrases, or excessive length. To address these issues, we employ LLaMA for chain-of-thought rewriting, which proves particularly effective at summarizing verbose captions and eliminating repetitive content. This refinement yields notable improvements: a 4% boost in MSR-VTT media-to-text retrieval and a 0.2% increase on ImageNet zero-shot accuracy.

Addressing Action Understanding Trade-offs However, we observe a 4% performance drop on the Kinetics dataset when training exclusively with synthetic captions. We attribute this degradation to the loss of hashtag information, which is crucial for action understanding but often not captured in synthetic captions. To recover

this performance while maintaining the benefits of synthetic captions, we introduce a siamese loss architecture operating on dual caption types:

- **Synthetic caption loss:** Computed on MMLLM-generated captions, where we occasionally sample a single sentence instead of the full caption (following the approach in [Bolya et al. \(2025\)](#)).
- **Hashtag caption loss:** Computed on aggregated hashtags from the original posts, preserving action-centric semantic information.

The siamese loss formulation allows the model to jointly learn from both caption types, successfully recovering the Kinetics performance while maintaining improvements on retrieval tasks. Through systematic experimentation with different loss weighting schemes, we find that a 1:1 ratio between synthetic caption loss and hashtag caption loss yields optimal results across all benchmarks.

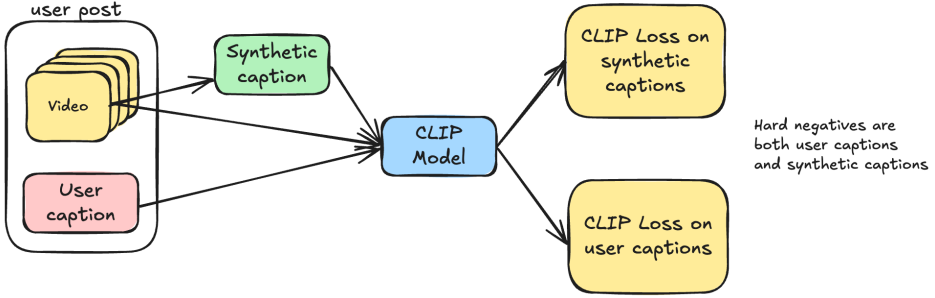


Figure 7 Siamese Loss

4.8 Attention pooling

We also tried attention pooling [Tang and Yang \(2024\)](#) in Xray, however we didn't see any significant gains by using attention pooling. This is most likely due to the scale of the data that has been used, which is 15B samples i.e. 8X as compared to PE [Bolya et al. \(2025\)](#), that we don't see any upsides. Similarly we tried RoPE [Su et al. \(2021\)](#) positional embedding as well, but that also didn't result into any significant gains.

4.9 Data augmentations

We implement a comprehensive data augmentation pipeline that builds upon established techniques while incorporating domain-specific enhancements. Our augmentation strategy adopts proven methods from Perception Encoder (PE) [Bolya et al. \(2025\)](#), including brightness and saturation jitter transformations, as well as horizontal flipping operations. Beyond these standard augmentations, we introduce Gaussian blurring as an additional preprocessing. This augmentation addresses a key challenge in real-world deployment scenarios where input imagery frequently exhibits substantial blurring or compression artifacts due to varying capture conditions. The complete augmentation pipeline is integrated with our self-supervised learning objective, creating a robust training regime that enhances model generalization capabilities. This comprehensive approach yields measurable performance improvements, contributing to a 0.3% accuracy gain on the Kinetics dataset. The incorporation of blur-specific augmentation proves particularly valuable for systems like Xray, where maintaining performance across diverse input quality conditions.

4.10 Native resolution Support with Variable aspect ratio

Contemporary vision encoders [Zhai et al. \(2023b\)](#); [Zhu et al. \(2025\)](#); [Bolya et al. \(2025\)](#) typically process full-resolution images and videos to achieve optimal performance, avoiding the information loss that results from cropping—a well-documented limitation in vision models. To address this challenge, we introduce a Variable Aspect Ratio Image Transform that preserves critical visual information while maintaining computational efficiency. Our proposed transform operates by intelligently resizing images along their larger dimension to conform to a specified target resolution while preserving the original aspect ratio. The method computes

optimal scaling factors for both width and height dimensions, ensuring proportional resizing that maintains the image’s geometric properties. Specifically, the transform resizes the input such that either the width or height completely occupies the target dimension, determined by whichever dimension is larger in the original image. To achieve the desired output resolution, the transform applies padding with a black background to fill the remaining spatial dimensions, with the resized image positioned at the center of the output frame. This approach effectively eliminates information loss that would otherwise occur through aggressive cropping or aspect ratio distortion, thereby preserving the visual integrity and semantic content of the input imagery. The Variable Aspect Ratio Image Transform thus enables our model to process diverse image formats without compromising on visual fidelity or computational performance, contributing to enhanced overall model effectiveness.

4.11 Knowledge Distillation

We employ a two-stage distillation strategy, first training large-scale 2B parameter EViT models as teachers, then distilling their knowledge into more efficient ViT-L student models. This approach enables us to achieve strong performance while maintaining computational efficiency for deployment.

Teacher Model Training We train separate teacher models for image and video modalities, each leveraging the strengths of our multi-modal training pipeline:

Image Teacher: We jointly train on the MetaCLIP and ViSE datasets to create a robust image teacher model. This combination leverages the diversity of MetaCLIP’s web-scale data with the high-quality social media captions from ViSE.

Video Teacher: For the video teacher, we combine ViSE image data with our video datasets using a 75:25 ratio. This mixed-modality training approach proves more effective than video-only training, as the model benefits from the rich visual concepts learned from images while developing temporal understanding from videos.

Distillation Strategy We distill both teacher models into ViT-L architectures for practical deployment. While we experimented with video-only teacher models, we observe superior results when the teacher is trained on a combined image-video recipe, validating our multi-modal training approach. The knowledge from large-scale joint training effectively transfers to smaller models, enabling efficient inference while preserving the representational quality learned at scale.

5 Results

We present comprehensive experimental results demonstrating the effectiveness of our approach trained on large-scale social media datasets. Our method achieves state-of-the-art performance across multiple challenging benchmarks, spanning image classification, video understanding, and cross-modal retrieval tasks. Our model establishes new state-of-the-art results on ImageNet [Deng et al. \(2009\)](#) classification, demonstrating superior performance compared to existing approaches. Furthermore, we evaluate robustness across challenging distribution shift scenarios, achieving state-of-the-art performance on established robustness benchmarks including ObjectNet [Barbu et al. \(2019\)](#) and ImageNet-Sketch [Wang et al. \(2019\)](#), which test model generalization under domain shift and stylistic variations. Extending our approach to video understanding through CLIP-style training methodologies, we achieve state-of-the-art results on standard video classification benchmarks, including Kinetics [Carreira and Zisserman \(2017\)](#) and HMDB51 [Kuehne et al. \(2011\)](#). These results demonstrate the effectiveness of our training paradigm for temporal reasoning and action recognition tasks. Our method demonstrates exceptional performance on cross-modal retrieval tasks, establishing state-of-the-art results on both MSRVTT [Xu et al. \(2016\)](#) and MSCOCO [Chen et al. \(2015\)](#) retrieval benchmarks. These results validate the quality of our learned joint embedding space for vision-language understanding. We conduct extensive evaluation on internal benchmarks to assess real-world applicability. Importantly, our analysis reveals a critical finding that challenges conventional assumptions: achieving state-of-the-art performance on established academic benchmarks does not necessarily translate to consistent improvements on internal evaluation metrics. This observation highlights the importance of comprehensive evaluation beyond standard benchmarks for practical deployment scenarios.

5.1 SOTA results

We now present our SOTA results across linear probing, zero shot and then retrieval on internal metrics.

5.1.1 Linear probing

Linear Probing Performance. Table 9 presents our comprehensive linear probing evaluation results. Our best-performing model, trained on the combination of ViSE and MetaCLIP datasets, achieves 89.3% accuracy on ImageNet linear probing, establishing a new state-of-the-art for this benchmark. Notably, our model trained exclusively on ViSE data without any external dataset augmentation achieves 89.1% accuracy, demonstrating the high quality and sufficiency of our curated training data.

Name	Encoder	ImageNet Top-1	ImageNet Top-5	Kinetics Top-1	Kinetics Top-5
PE-L	PE-L	87.64	98.53	72.1	90.32
PE-G	PE-G	89.22	98.53	76.68	92.79
SiGLIP-L	ViTL-16	83.10	-	-	-
DiNO-v3	7B	88.10	-	68.10	84.51
X-Ray ViTL-16	ViTL-16	87.94	98.51	-	-
X-Ray Image EViT-2b	EViT-2b	89.30	97.37	-	-
X-Ray Visual EViT-2b	EViT-2b	88.10	96.37	78.10	98.37
X-Ray Image (ViSE)	EViT-2b	89.19	97.14	-	-

Table 9 Model and ImageNet Linear probing performance metrics.

Name	Encoder	Kinetics Top-1	Kinetics Top-5	UCF101 Top-1	UCF101 Top-5	HMDB51 Top-1	HMDB51 Top-5
PE-G	PE-G	76.68	92.79	96.99	99.89	77.50	95.54
SiGLIP 2	ViT-g/16	51.15	69.96	55.31	68.93	47.83	73.87
DiNO-v3	ViT-H	70.19	88.36	94.30	99.52	65.58	91.75
X-Ray Visual	EViT-2b	78.10	98.37	98.24	99.86	74.69	94.21

Table 10 Model and Video Classification Linear probing performance metrics.

Computational Efficiency. A key advantage of our approach lies in its computational efficiency. Our models demonstrate $4\times$ improved efficiency compared to standard vision encoders, including Perception Encoder [Bolya et al. \(2025\)](#), CLIP [Radford et al. \(2021a\)](#), and DiNO [Caron et al. \(2021\)](#); [Oquab et al. \(2023\)](#), by utilizing only 25% of the visual tokens during processing. This efficiency gain enables our method to achieve the dual objectives of scalability and state-of-the-art performance without compromising accuracy.

Video Classification Results. For video understanding tasks, our approach achieves 78.1% Top-1 accuracy on the Kinetics dataset, establishing state-of-the-art performance for video classification. Our method demonstrates substantial improvements over existing approaches, with gains of $+1.5\%$ over Perception Encoder and $+10\%$ over the DiNO vision encoder. We attribute these significant improvements on Kinetics to our comprehensive training methodology, which leverages over 5 billion video samples across a carefully designed three-stage training curriculum. This large-scale video training enables our model to capture rich temporal dynamics and complex motion patterns essential for robust video understanding.

5.1.2 Zero Shot results

Zero-Shot Evaluation. Table 12 presents our comprehensive zero-shot evaluation results, demonstrating state-of-the-art performance across multiple benchmarks. Our method achieves superior zero-shot performance on both ImageNet Top-1 and MS-COCO Top-1 metrics, with notable improvements of $+1.05\%$ on MS-COCO Top-1 and $+0.25\%$ on ImageNet Top-1 compared to existing approaches. To achieve these results, we employ a knowledge distillation strategy that transfers learned representations from our 2B parameter models to more efficient ViT-H and ViT-L architectures. This distillation process leverages synthetic captions generated using LLaMA-4 and ViSE-enhanced LLM-generated captions, which prove instrumental in improving zero-shot performance. While synthetic caption augmentation demonstrates clear benefits for zero-shot evaluation,

Table 11 Classification accuracy of linear probes trained on ImageNet1k with frozen backbones. Weakly- and self-supervised models are evaluated with image resolution adapted to 1024 patch tokens (i.e., 448×448 for patch size 14, 512×512 for patch size 16). For reference, we also list results from Dehghani et al. (2023) using a different evaluation protocol (marked with *). Xray is evaluated on 336 resolution with only 288 active tokens; making it more efficient than the contemporary models, while getting improved results.

Method	ViT	ImageNet			Rendition		Hard		
		Val	V2	ReaL	R	S	A	C \downarrow	Obj.
Supervised backbones									
Zhai et al. (2022a)*	G/14	89.0	81.3	90.6	91.7	—	78.8	—	69.6
Chen et al. (2023)*	e/14	89.3	82.5	90.7	94.3	—	81.6	—	71.5
Dehghani et al. (2023)*	22B/14	89.5	83.2	90.9	94.3	—	83.8	—	74.3
Agglomerative backbones									
AM-RADIOv2.5	g/14	88.0	80.2	90.3	83.8	67.1	81.3	27.1	68.4
Weakly-supervised backbones									
PEcore	G/14	89.3	81.6	90.4	92.2	71.9	89.0	22.7	80.2
SigLIP 2	g/16	89.1	81.6	90.5	92.2	71.8	84.6	30.0	78.6
AIMv2	3B/14	87.9	79.5	89.7	82.3	67.1	74.5	29.5	69.0
EVA-CLIP	18B/14	87.9	79.3	89.5	85.2	64.0	81.6	33.0	71.9
Self-supervised backbones									
Web-DINO	7B/14	85.9	77.1	88.6	75.6	64.0	71.6	31.2	69.7
Franca	g/14	84.8	75.3	89.2	67.6	49.5	56.5	40.0	54.5
DINOv2	g/14	87.3	79.5	89.9	81.1	65.4	81.7	24.1	66.4
DINOv3	7B/16	88.4	81.4	90.4	91.1	71.3	86.9	19.6	79.0
Ours									
Xray	EViT-2B	89.3	81.4	-	94.4	72.9	88.9	-	83.8

we note that improvements in zero-shot metrics do not necessarily correlate with enhanced performance on internal retrieval benchmarks, as detailed in the subsequent section. We also report results on new country211, fgvc-aircraft, food etc in Table 14. We see that our OOD generalization is pretty strong and we SOTA results on ImageNet-Sketch Wang et al. (2019), ImageNet rendidition. Interestingly on some datasets like sun397 and resisc45, our results are not SOTA; this primarily is due to difference in data distibution between academic datasets and large scale industry datasets.

5.2 Transfer learning results

We also do transfer learning by evaluating our model on linear probing in transfer learning setting.

Name	Encoder	Parameter Count	MSCOCO Img-Text r@1	MSCOCO Text-Img r@1	ImageNet Top-1	ImageNet Top-5
PE	ViTL	300M	72.75	54.21	83.08	97.22
SigLIP	ViTL	300M	71.40	55.30	83.10	97.20
DiNO-v3.txt	ViT-7B	7B	63.7	45.6	82.3	96.21
X-Ray Visual	ViTL	300M	73.21	55.06	83.07	97.28
X-Ray Visual	ViTH	832M	73.83	55.11	83.33	97.37

Table 12 Model and MSCOCO/ImageNet Zero-Shot performance metrics.

5.2.1 MMEB Results

We evaluate our approach on the MMEB validation set through direct zero-shot inference without any fine-tuning on the MMEB training data. As demonstrated in Table 13, our Xray model achieves state-of-the-art results within the 2B parameter model category, often surpassing comparable methods by substantial margins. Specifically, we observe significant improvements of +8.1% on ObjectNet, +15.5% on ImageNet-Adversarial, and +4.1% on ImageNet Rendition compared to the nearest competing approaches. These substantial improvements on adversarial datasets highlight the robust generalization capabilities of our Xray model beyond its training distribution. This generalization behavior represents a critical advancement for production deployment scenarios involving large-scale Meta traffic, where models frequently encounter out-of-distribution (OOD) imagery. The strong performance on adversarial benchmarks validates the practical utility of our approach for real-world applications.

In Table 15 we show results on video zeros shot datasets. We get +5-6% above the best multi-modal models and show promising gains while being 20x smaller than MMLM’s.

Models	Model Size (B)	Image CLS	SUN397	ObjectNet	Country211	Place365	ImageNet-1K	ImageNet-A	ImageNet-R
XRay Model EViT-2B	2.4	66.8	71.9	79.4	44.2	44.8	79.5	68.6	95.3
XRay Model ViT-H	0.6B	66.1	73.5	79.6	36.0	45.7	83.3	65.2	93.6
Ops-MM-embedding-v1-2B	2.21	65.1	80.7	68.4	28.6	43.9	81.1	53.1	91.2
RzenEmbed-v1-2B	2.21	61.2	78.4	71.3	24.5	41.3	80.9	49.5	84.8
VLM2Vec-V2.0-Qwen2VL-2B	2.21	58.9	71.0	65.2	25.2	35.9	80.8	47.4	89.3
VLM2Vec-V1-Qwen2VL-2B	2.21	54.9	73.8	37.1	21.5	35.3	77.5	50.9	84.7
gme-Qwen2-VL-2B-Instruct	2.21	52.3	67.3	70.6	26.5	35.8	58.3	28.8	78.6
interestFM-UIR-CAFe-0.5B	0.894	51.6	68.8	51.0	11.3	37.4	64.6	38.1	86.4
colpali-v1.3	2.92	38.5	56.1	45.6	6.0	27.5	42.4	14.9	64.6

Table 13 MMEB Performance Comparison of Models

	cars	country211	fgvc-aircraft	food101	imagenet-a	imagenet-r	imagenet1k	imagenet-sketch	imagenetv2	objectnet	sun397	vtab-flowers	vtab-pets	vtab-resisc45
KD 2B to ViT-H, Vise	0.85040	0.34290	0.33710	0.96230	0.83980	0.93560	0.82200	0.85040	0.76440	0.76910	0.75120	0.89700	0.96810	0.63820
KD 2B to ViT-H, M+V+L4	0.93710	0.39660	0.68150	0.96250	0.86260	0.94740	0.83330	0.93710	0.77970	0.81630	0.77350	0.88690	0.96400	0.71490
MetaCLIP+ViSE	0.90027	0.40137	0.41016	0.97012	0.86641	0.94458	0.82914	0.77764	0.72584	0.82221	0.74619	0.86507	0.97339	0.66376
Only ViSE	0.90027	0.40137	0.41016	0.97012	0.86641	0.94458	0.82914	0.77764	0.72584	0.82221	0.74619	0.86507	0.97339	0.66376
LiT-22B	-	-	-	-	0.901	0.960	0.859	-	0.809	0.876	-	-	-	-
SigLIP-B/16	0.908	0.440	0.159	0.916	0.451	0.902	0.762	0.679	0.695	0.707	-	0.852	0.942	0.646
SigLIP2-B/16	0.934	0.548	0.192	0.928	0.550	0.917	0.782	0.689	0.731	0.736	-	0.857	0.954	0.711
PEcore B	0.921	0.570	0.305	0.925	0.624	0.887	0.784	0.661	0.750	0.719	-	0.865	0.946	0.727
SigLIP-L/16	0.948	0.532	0.247	0.956	0.765	0.950	0.736	0.744	0.956	0.894	0.968	0.948	0.532	0.679
SigLIP2-L/16	0.958	0.670	0.316	0.961	0.843	0.957	0.755	0.784	0.961	0.900	0.964	0.958	0.670	0.755
PEcore L	0.937	0.678	0.456	0.962	0.890	0.952	0.734	0.800	0.962	0.872	0.964	0.937	0.678	0.757
DFN-H+	0.960	0.725	0.379	0.962	0.796	0.936	0.733	0.805	0.962	0.916	0.968	0.960	0.725	0.759
InternVL-C	0.944	0.533	0.351	0.953	0.838	0.957	0.743	0.764	0.953	0.858	0.963	0.944	0.533	0.744
EVA 1SB	0.949	0.597	0.431	0.958	0.873	0.957	0.747	0.788	0.958	0.860	0.961	0.949	0.597	0.769
EVA 1SB+	-	-	-	-	0.889	0.956	0.743	-	-	-	-	-	-	-
SigLIP2-g-opt	0.959	0.736	0.401	0.970	0.905	0.966	0.774	0.810	0.970	0.915	0.978	0.959	0.736	0.759
PEcore G (image only)	0.946	0.767	0.573	0.966	0.912	0.961	0.761	0.827	0.966	0.910	0.964	0.946	0.767	0.718
PEcore G	0.947	0.782	0.576	0.969	0.926	0.965	0.765	0.837	0.969	0.914	0.969	0.947	0.782	0.758

Table 14 Performance of models on Transfer learning.

Models	Backbone	Overall	UCF101	Breakfast	K-700	HMDB51	sth-sth V2
Qwen2 VL	7 Billion	57.6	78.6	37.200	55.6	63.9	53
X-Ray visual	400M	63.0	85.5	41.8	66.7	57.8	54.2

Table 15 Comparison of model performance across MMEB Video benchmarks.

5.3 Internal metrics

Internal Evaluation on Benchmarks. Beyond standard academic benchmarks, we conduct extensive evaluation on internal reels-to-ads and FB search retrieval tasks, which serve as critical indicators of real-world performance. These benchmarks provide essential insights into model behavior on practical scenarios.

Dataset and Evaluation Protocol. Our ads evaluation encompasses ad-to-ad and Instagram/Facebook reels-to-ads retrieval datasets, designed to assess the model’s ability to determine semantic similarity between advertisements and social media content. Ground-truth similarity labels are established through majority vote consensus from a minimum of three independent human annotators, ensuring reliable evaluation standards.

We evaluate semantic similarity by computing cosine similarity between learned embeddings, providing a direct measure of representational quality. FB search retrieval evaluation measures the model’s ability to retrieve the corresponding image or text. User click through rate is used to remove noisy image and text FB post pairs.

Performance Analysis. Table 16 and 17 presents our comprehensive results on these internal benchmarks. Compared to models trained exclusively on external datasets, XRay demonstrates substantial performance improvements across all evaluation scenarios.

Domain Shift Analysis. A critical finding from our evaluation reveals that state-of-the-art vision encoders, including Perception Encoder (PE) and DiNO, exhibit significant performance degradation under domain shift conditions. While XRay achieves a +1.8 AUC improvement on same-domain ads-to-ads retrieval, the performance gap becomes dramatically more pronounced in cross-domain scenarios. Specifically, XRay achieves remarkable improvements of +10.8% on Instagram reels-to-ads retrieval and +10.2% on Facebook reels-to-ads retrieval compared to the Perception Encoder baseline. Although XRay ViT-L variant and PE-L have similar MSCOCO retrieval performance, XRay achieves +2% gain on FB search metrics.

Implications for Real-World Deployment. These results highlight a fundamental limitation in current state-of-the-art vision encoders: substantial performance degradation when confronted with real-world out-of-distribution (OOD) scenarios. This observation underscores the critical need for incorporating more diverse training data in vision encoder development. While training on curated, clean datasets may yield strong performance on academic benchmarks, such approaches fail to generalize effectively to practical use cases—a phenomenon well-documented in large language models but previously underexplored in vision encoders.

LLM-based Text Encoders. We investigate the effectiveness of employing large language models as text encoders in our multimodal framework. Specifically, we replace conventional text encoders with LLaMA [Touvron et al. \(2023b\)](#), leveraging its enhanced linguistic representation capabilities for improved cross-modal understanding. Our experimental analysis reveals that LLM-based text encoding yields substantially stronger overall performance compared to standard text encoding approaches. While academic benchmark evaluations did not demonstrate significant improvements, we observed considerable gains on internal evaluation metrics. This discrepancy between academic and internal benchmark performance further reinforces the critical importance of employing generalized, robust models for practical deployment scenarios. The superior performance of LLM-based text encoding on internal metrics suggests that the richer linguistic representations learned by large-scale language models provide enhanced semantic alignment capabilities, particularly beneficial for real-world applications involving diverse and complex textual content.

We also evaluated our model on CIFAR dataset which is a low resolution dataset. We found our results not to be SOTA, primarily due to mismatch of training domains and resolution. However that doesn’t deter from getting good results on real world datasets.

Name	Encoder	Ad to Ad AUC	IG Reels to Ads AUC	FB Reels to Ads AUC
XRay-LLM2CLIP	ViTL-16	90.21	67.03	77.7
PE-L	ViTL-16	88.54	56.14	67.36
PE-G	ViT-G	89.67	63.22	69.86
DinoV2 with text	ViTL-14	84.35	53.69	61.4

Table 16 Reels and Ads performance metrics

Name	Encoder	COCO Img-Text r@1	COCO Text-Img r@1	FB Img-Text r@1	FB Text-Img r@1
XRay Model	ViTL-16	73.21	55.06	52.06	48.9
PE-L	ViTL-16	75.9	57.1	49.39	47.02

Table 17 FB Search retrieval metrics

6 Practical Deployment and Applications

This section examines the practical deployment considerations and real-world applications of our proposed model, highlighting integration strategies and performance trade-offs.

6.1 Applications

Our model serves as a component across multiple production systems, providing robust visual representations for diverse downstream tasks. The primary application domain centers on recommendation systems, where the core objective involves retrieving the most semantically relevant videos given input images or videos. In recommendation frameworks, the system leverages user interaction history to retrieve contextually appropriate content conditioned on previous engagement patterns. Additional deployment scenarios include bidirectional ads-to-reels retrieval systems and comprehensive ads-to-ads matching pipelines. These applications demonstrate the versatility of our learned representations across diverse content modalities.

6.2 Linear Adapter Integration

A particularly effective deployment strategy involves training lightweight linear adapters on top of our pre-trained embeddings for specialized downstream tasks. This approach enables rapid task-specific adaptation while preserving the core representational capabilities. For instance, we demonstrate this methodology for AI-generated content detection, where we utilize LLaMA [Touvron et al. \(2023b\)](#) for data annotation and subsequently train linear classifiers for content authenticity assessment. This approach achieves performance comparable to multimodal large language models while requiring only a fraction of the computational resources.

6.3 Dimensionality Reduction for Scalable Deployment

The full-dimensional embeddings from ViT-H (1280d) and ViT-L (1024d) models present significant computational and storage challenges. To address scalability requirements, we implement 100-dimensional projection layers that substantially reduce costs while maintaining reasonable performance. Empirical evaluation reveals that this dimensionality reduction incurs approximately 4% performance degradation on ImageNet classification and a more substantial 5% drop on Kinetics video classification. Despite these performance trade-offs, the cost-to-performance ratio strongly favors the 100-dimensional embeddings.

6.4 Quantization-Based Compression

As an alternative to dimensionality reduction, we explore quantization techniques for embedding compression. Our quantization pipeline reduces embeddings to int8 precision, achieving superior performance compared to 100-dimensional projections while maintaining storage efficiency. Quantized embeddings demonstrate notably smaller performance degradation, with approximately 3% accuracy reduction on ImageNet compared to full-precision representations. However, practical deployment of quantized embeddings presents integration challenges, as downstream client systems require specialized support and special care needs to be taken to use quantized embedding.

6.5 Similarity focussed models

We also build specialized models for focussing on near duplicate detection task. Our large scale we saw that current Xray models performed pretty well on near duplicate detection. However we were able to improve upon it by making a new model, where we started by pre-training on MAE [He et al. \(2022\)](#) and then we followed by SimCLR [Chen et al. \(2020\)](#). We saw combination of these models gave the best results for near duplicates.

6.6 Semantic ID

Semantic IDs are discrete tokenizers derived from embeddings. They play a key role in recommendation systems, where MTML models are typically designed to consume both continuous and sparse ID features. Unlike traditional unique item IDs, semantic IDs enable models to generalize to unseen or similar items,

promote balanced learning, and capture hierarchical content structures through a shared vocabulary of tokens generated from item content. We experimented with two variants of Xray-Visual tokenizers built upon VQVAE-V2 (Razavi et al., 2019).

The first variant adopts residual quantization (Lee et al., 2022). Given an Xray embedding as input, the model encodes it and performs a K -level hierarchical vector quantization. At each level, the input residual vector is matched against a codebook by cosine similarity, producing a discrete codeword and a residual that is passed to the next level. The K selected codeword embeddings are then summed to reconstruct the input. This hierarchical quantization scheme yields compact and expressive semantic IDs that capture both coarse- and fine-grained content structures.

The second variant employs product quantization (Hou et al., 2025). Instead of applying quantization sequentially, the model splits the encoded Xray embedding into K chunks, each of which undergoes vector quantization in parallel. The resulting K codeword embeddings are concatenated to reconstruct the input. This parallel quantization scheme produces semantic IDs that represent distinct topics within the same input.

In practice, we found that combining the two semantic ID variants provides complementary benefits for downstream applications. To stabilize training and improve codebook utilization in both variants, we follow VQVAE-V2 (Razavi et al., 2019) and update the codebook vectors using an exponential moving average (EMA) rather than gradient-based optimization. This EMA update mitigates codebook collapse and promotes smoother convergence.

7 Related Works

7.1 CLIP

There has been many approaches proposed for pre-training the ViT for vision-language alignment. CLIP (Radford et al., 2021a; Jia et al., 2021) becomes the popular choice, due to its superior performance on multimodal understanding as studied in Tong et al. (2024). Other methods leverage sigmoid loss like SigLIP (Zhai et al., 2023b; Tschanen et al., 2025) or captioning loss like Cappa (Tschanen et al., 2024) are also popular; LocCa (Wan et al., 2024) further incorporates bounding box coordinates. However, they need to train a full encoder-decoder transformer with smaller batch sizes, which is less efficient than CLIP. Also, the vision embeddings are not directly aligned with languages, so more limited for search or retrieval tasks. Therefore we focus on comparing against works on the CLIP approach.

To enhance the fine-grained understanding of vision embeddings, some recent works (Naeem et al., 2023; Bica et al., 2024; Dong et al., 2023) combine localization-enhancing unsupervised objectives with the CLIP loss. Alpha-CLIP (Sun et al., 2024) shows that the SAM (Kirillov et al., 2023) can provide useful conditions for CLIP. Another work, CLOC (Chen et al., 2025) uses supervision on large-scale explicit pseudo-labeled detection data to train the CLIP encoder enable better local feature extraction. AIM-v2 (Fini et al., 2025) proposed to combine pixel-level reconstruction loss with the CLIP loss. Differently, we inject the localization knowledge via our proposed multi-stage training recipe with MAE to without any external supervision.

Another promising direction is enhancing the quality of the image captions through LLM re-writing (Lai et al., 2025; Nguyen et al., 2023), which has been proven improving the retrieval performance. We also incorporate high-quality synthetic captions on the native social media domains that not only enrich the visual information but also better capture users’ interests and intention.

7.2 Self-Supervised Learning

Contrastive learning has emerged as a foundational approach in self-supervised computer vision, enabling models to learn general-purpose representations without the need for labeled data. Early works such as SimCLR Chen et al. (2020), MoCo He et al. (2020), and DINO Caron et al. (2021) demonstrated that contrastive objectives—by enforcing invariance to data augmentations and leveraging negative samples—can achieve state-of-the-art performance on image recognition tasks [van den Oord et al. (2018); Hénaff et al. (2020); He et al. (2020); Tian et al. (2020); Chuang et al. (2020); Chen et al. (2021); . These methods were initially developed for ConvNet backbones, but subsequent research showed that, with proper architectural

tuning, they could be successfully adapted to Vision Transformers (ViT) [Dosovitskiy et al. \(2021\)](#). The key idea in contrastive learning is to spread the learned embeddings uniformly on the sphere, using negative samples to avoid trivial solutions [Robinson et al., 2021](#); [Mishra et al., 2022](#); [Ge et al., 2021](#); [Wang et al., 2019](#) .

7.3 Masked Image Modeling and Autoencoding Methods

The advent of Vision Transformers (ViT) [Dosovitskiy et al. \(2021\)](#) has also spurred the development of masked image modeling techniques, which take inspiration from masked language modeling in NLP ([Devlin et al., 2018](#); [Devlin, 2019](#); [Touvron et al., 2023b](#)) . In this paradigm, models learn to reconstruct masked portions of input images, thereby capturing rich spatial statistical dependencies. Notable methods such as MAE (Masked Autoencoder) [He et al. \(2022\)](#), BEiT [Bao et al. \(2022\)](#) , and related approaches [Chen et al. \(2022\)](#); [Xie et al. \(2022\)](#) have shown that it is possible to pre-train ViTs efficiently by omitting masked tokens from the encoder, resulting in significant computational savings. Unlike contrastive learning, autoencoders encourage information preservation in the latent representations, which can lead to different feature learning dynamics. The efficiency and scalability of masked image modeling have made it a popular choice for large-scale vision pre-training, and our work similarly leverages these advances to build robust multimodal models.

References

Mido Assran, Adrien Bardes, David Fan, Quentin Garrido, Russell Howes, Mojtaba, Komeili, Matthew Muckley, Ammar Rizvi, Claire Roberts, Koustuv Sinha, Artem Zhulus, Sergio Arnaud, Abha Gejji, Ada Martin, Francois Robert Hogan, Daniel Dugas, Piotr Bojanowski, Vasil Khalidov, Patrick Labatut, Francisco Massa, Marc Szafraniec, Kapil Krishnakumar, Yong Li, Xiaodong Ma, Sarath Chandar, Franziska Meier, Yann LeCun, Michael Rabbat, and Nicolas Ballas. V-jepa 2: Self-supervised video models enable understanding, prediction and planning, 2025. <https://arxiv.org/abs/2506.09985>.

Hangbo Bao, Li Dong, and Furu Wei. BEiT: BERT pre-training of image transformers. In *ICLR*, 2022.

Andrei Barbu, David Mayo, Julian Alverio, William Luo, Christopher Wang, Dan Gutfreund, Joshua B. Tenenbaum, and Boris Katz. Objectnet: A large-scale bias-controlled dataset for pushing the limits of object recognition models. In *Neural Information Processing Systems*, 2019. <https://api.semanticscholar.org/CorpusID:202777185>.

Ioana Bica, Anastasija Ilić, Matthias Bauer, Goker Erdogan, Matko Bošnjak, Christos Kaplanis, Alexey A Gritsenko, Matthias Minderer, Charles Blundell, Razvan Pascanu, et al. Improving fine-grained understanding in image-text pre-training. *arXiv preprint arXiv:2401.09865*, 2024.

Daniel Bolya, Cheng-Yang Fu, Xiaoliang Dai, Peizhao Zhang, Christoph Feichtenhofer, and Judy Hoffman. Token merging: Your vit but faster. *ArXiv*, abs/2210.09461, 2022. <https://api.semanticscholar.org/CorpusID:252968113>.

Daniel Bolya, Po-Yao Huang, Peize Sun, Jang Hyun Cho, Andrea Madotto, Chen Wei, Tengyu Ma, Jiale Zhi, Jathushan Rajasegaran, Hanoona Rasheed, Junke Wang, Marco Monteiro, Hu Xu, Shiyu Dong, Nikhila Ravi, Daniel Li, Piotr Dollár, and Christoph Feichtenhofer. Perception encoder: The best visual embeddings are not at the output of the network. *arXiv:2504.13181*, 2025.

Tom Brown, Benjamin Mann, Nick Ryder, Melanie Subbiah, Jared D Kaplan, Prafulla Dhariwal, Arvind Neelakantan, Pranav Shyam, Girish Sastry, Amanda Askell, et al. Language models are few-shot learners. In *NeurIPS*, 2020.

Tom B Brown. Language models are few-shot learners. *arXiv preprint arXiv:2005.14165*, 2020.

Mathilde Caron, Hugo Touvron, Ishan Misra, Hervé Jégou, Julien Mairal, Piotr Bojanowski, and Armand Joulin. Emerging properties in self-supervised vision transformers. In *Proceedings of the IEEE/CVF International Conference on Computer Vision (ICCV)*, pages 9650–9660, 2021.

João Carreira and Andrew Zisserman. Quo vadis, action recognition? a new model and the kinetics dataset. *2017 IEEE Conference on Computer Vision and Pattern Recognition (CVPR)*, pages 4724–4733, 2017. <https://api.semanticscholar.org/CorpusID:206596127>.

Hong-You Chen, Zhengfeng Lai, Haotian Zhang, Xinze Wang, Marcin Eichner, Keen You, Meng Cao, Bowen Zhang, Yinfei Yang, and Zhe Gan. Contrastive localized language-image pre-training. In *Forty-second International Conference on Machine Learning*, 2025. <https://openreview.net/forum?id=sGQEOXlezg>.

Ting Chen, Simon Kornblith, Mohammad Norouzi, and Geoffrey Hinton. A simple framework for contrastive learning of visual representations. In *International Conference on Machine Learning*, pages 1597–1607. PMLR, 2020.

Xiangning Chen, Chen Liang, Da Huang, Esteban Real, Kaiyuan Wang, Yao Liu, Hieu Pham, Xuanyi Dong, Thang Luong, Cho-Jui Hsieh, Yifeng Lu, and Quoc V. Le. Symbolic discovery of optimization algorithms. *ArXiv*, abs/2302.06675, 2023. <https://api.semanticscholar.org/CorpusID:256846990>.

Xiaokang Chen, Mingyu Ding, Xiaodi Wang, Ying Xin, Shentong Mo, Yunhao Wang, Shumin Han, Ping Luo, Gang Zeng, and Jingdong Wang. Context autoencoder for self-supervised representation learning. In *preprint arXiv:2202.03026*, 2022.

Xinlei Chen, Hao Fang, Tsung-Yi Lin, Ramakrishna Vedantam, Saurabh Gupta, Piotr Dollár, and C Lawrence Zitnick. Microsoft coco captions: Data collection and evaluation server. *arXiv preprint arXiv:1504.00325*, 2015.

Xinlei Chen, Saining Xie, and Kaiming He. An empirical study of training self-supervised vision transformers. In *ICCV*, pages 9640–9649, 2021.

Xinlei Chen, Zhuang Liu, Saining Xie, and Kaiming He. Deconstructing denoising diffusion models for self-supervised learning. *arXiv preprint arXiv:2401.14404*, 2024.

Ching-Yao Chuang, Joshua Robinson, Yen-Chen Lin, Antonio Torralba, and Stefanie Jegelka. Debiased contrastive learning. In *NEURIPS*, volume 33, pages 8765–8775, 2020.

Yung-Sung Chuang, Yang Li, Dong Wang, Ching-Feng Yeh, Kehan Lyu, Ramya Raghavendra, James Glass, Lifei Huang, Jason Weston, Luke Zettlemoyer, Xinlei Chen, Zhuang Liu, Saining Xie, Wen tau Yih, Shang-Wen Li, and Hu Xu. Metaclip 2: A worldwide scaling recipe. *arXiv preprint arXiv:2507.22062*, 2025.

Timothée Darcet, Maxime Oquab, Julien Mairal, and Piotr Bojanowski. Vision transformers need registers. *ArXiv*, abs/2309.16588, 2023. <https://api.semanticscholar.org/CorpusID:263134283>.

Jia Deng, Wei Dong, Richard Socher, Li-Jia Li, Kai Li, and Li Fei-Fei. Imagenet: A large-scale hierarchical image database. In *CVPR*, 2009.

Jacob Devlin. Bert: Pre-training of deep bidirectional transformers for language understanding. In *NAACL*, 2019.

Jacob Devlin, Ming-Wei Chang, Kenton Lee, and Kristina Toutanova. BERT: Pre-training of deep bidirectional transformers for language understanding. In *NAACL*, 2018.

Xiaoyi Dong, Jianmin Bao, Yinglin Zheng, Ting Zhang, Dongdong Chen, Hao Yang, Ming Zeng, Weiming Zhang, Lu Yuan, Dong Chen, et al. Maskclip: Masked self-distillation advances contrastive language-image pretraining. In *Proceedings of the IEEE/CVF Conference on Computer Vision and Pattern Recognition*, pages 10995–11005, 2023.

Alexey Dosovitskiy, Lucas Beyer, Alexander Kolesnikov, Dirk Weissenborn, Xiaohua Zhai, Thomas Unterthiner, Mostafa Dehghani, Matthias Minderer, Georg Heigold, Sylvain Gelly, Jakob Uszkoreit, and Neil Houlsby. An image is worth 16x16 words: Transformers for image recognition at scale. In *International Conference on Learning Representations (ICLR)*, 2021.

Lijie Fan, Dilip Krishnan, Phillip Isola, Dina Katabi, and Yonglong Tian. Improving clip training with language rewrites. *ArXiv*, abs/2305.20088, 2023a. <https://api.semanticscholar.org/CorpusID:258987272>.

Lijie Fan, Dilip Krishnan, Phillip Isola, Dina Katabi, and Yonglong Tian. Improving clip training with language rewrites, 2023b. <https://arxiv.org/abs/2305.20088>.

Christoph Feichtenhofer, Haoqi Fan, Yanghao Li, and Kaiming He. Masked autoencoders as spatiotemporal learners, 2022. <https://arxiv.org/abs/2205.09113>.

Enrico Fini, Mustafa Shukor, Xiuju Li, Philipp Dufter, Michal Klein, David Haldimann, Sai Aitharaju, Victor G Turrisi da Costa, Louis Béthune, Zhe Gan, et al. Multimodal autoregressive pre-training of large vision encoders. In *Proceedings of the Computer Vision and Pattern Recognition Conference*, pages 9641–9654, 2025.

Tianyu Gao, Xingcheng Yao, and Danqi Chen. Simcse: Simple contrastive learning of sentence embeddings. *ArXiv*, abs/2104.08821, 2021. <https://api.semanticscholar.org/CorpusID:233296292>.

Songwei Ge, Shlok Kumar Mishra, Haohan Wang, Chun-Liang Li, and David Jacobs. Robust contrastive learning using negative samples with diminished semantics. In *NEURIPS*, volume abs/2110.14189, 2021.

Deepti Ghadiyaram, Matt Feiszli, Du Tran, Xuetong Yan, Heng Wang, and Dhruv Kumar Mahajan. Large-scale weakly-supervised pre-training for video action recognition. *2019 IEEE/CVF Conference on Computer Vision and Pattern Recognition (CVPR)*, pages 12038–12047, 2019. <https://api.semanticscholar.org/CorpusID:143423501>.

Aaron Grattafiori, Abhimanyu Dubey, Abhinav Jauhri, Abhinav Pandey, Abhishek Kadian, Ahmad Al-Dahle, Aiesha Letman, Akhil Mathur, Alan Schelten, Alex Vaughan, Amy Yang, Angela Fan, Anirudh Goyal, Anthony Hartshorn, Aobo Yang, Archi Mitra, Archie Sravankumar, Artem Korenev, Arthur Hinsvark, Arun Rao, Aston Zhang, Aurelien Rodriguez, Austen Gregerson, Ava Spataru, Baptiste Roziere, Bethany Biron, Binh Tang, Bobbie Chern, Charlotte Caucheteux, Chaya Nayak, Chloe Bi, Chris Marra, Chris McConnell, Christian Keller, Christophe Touret, Chunyang Wu, Corinne Wong, Cristian Canton Ferrer, Cyrus Nikolaidis, Damien Allonsius, Daniel Song, Danielle Pintz, Danny Livshits, Danny Wyatt, David Esiobu, Dhruv Choudhary, Dhruv Mahajan, Diego Garcia-Olano, Diego Perino, Dieuwke Hupkes, Egor Lakomkin, Ehab AlBadawy, Elina Lobanova, Emily Dinan, Eric Michael Smith, Filip Radenovic, Francisco Guzmán, Frank Zhang, Gabriel Synnaeve, Gabrielle Lee, Georgia Lewis Anderson, Govind Thattai, Graeme Nail, Gregoire Mialon, Guan Pang, Guillem Cucurell, Hailey Nguyen, Hannah Korevaar, Hu Xu, Hugo Touvron, Iliyan Zarov, Imanol Arrieta Ibarra, Isabel Kloumann, Ishan Misra, Ivan Evtimov, Jack Zhang, Jade Copet, Jaewon Lee, Jan Geffert, Jana Vranes, Jason Park, Jay Mahadeokar, Jeet Shah, Jelmer van der Linde, Jennifer Billock, Jenny Hong, Jenya Lee, Jeremy Fu, Jianfeng Chi, Jianyu Huang, Jiawen Liu, Jie Wang, Jiecao Yu, Joanna Bitton, Joe Spisak, Jongsoo Park, Joseph Rocca, Joshua Johnstun, Joshua Saxe, Junteng Jia, Kalyan Vasuden Alwala, Karthik Prasad, Kartikeya Upasani, Kate Plawiak, Ke Li, Kenneth Heafield, Kevin Stone, Khalid El-Arini, Krithika Iyer, Kshitiz Malik, Kuenley Chiu, Kunal Bhalla, Kushal Lakhota, Lauren Rantala-Yeary, Laurens van der Maaten, Lawrence Chen, Liang Tan, Liz Jenkins, Louis Martin, Lovish Madaan, Lubo Malo, Lukas Blecher, Lukas Landzaat, Luke de Oliveira, Madeline Muzzi, Mahesh Pasupuleti, Mannat Singh, Manohar Paluri, Marcin Kardas, Maria Tsimpoukelli, Mathew Oldham, Mathieu Rita, Maya Pavlova, Melanie Kambadur, Mike Lewis,

Min Si, Mitesh Kumar Singh, Mona Hassan, Naman Goyal, Narjes Torabi, Nikolay Bashlykov, Nikolay Bogoychev, Niladri Chatterji, Ning Zhang, Olivier Duchenne, Onur Çelebi, Patrick Alrassy, Pengchuan Zhang, Pengwei Li, Petar Vasic, Peter Weng, Prajjwal Bhargava, Pratik Dubal, Praveen Krishnan, Punit Singh Koura, Puxin Xu, Qing He, Qingxiao Dong, Ragavan Srinivasan, Raj Ganapathy, Ramon Calderer, Ricardo Silveira Cabral, Robert Stojnic, Roberta Raileanu, Rohan Maheswari, Rohit Girdhar, Rohit Patel, Romain Sauvestre, Ronnie Polidoro, Roshan Sumbaly, Ross Taylor, Ruan Silva, Rui Hou, Rui Wang, Saghar Hosseini, Sahana Chennabasappa, Sanjay Singh, Sean Bell, Seohyun Sonia Kim, Sergey Edunov, Shaoliang Nie, Sharan Narang, Sharath Raparthy, Sheng Shen, Shengye Wan, Shruti Bhosale, Shun Zhang, Simon Vandenhende, Soumya Batra, Spencer Whitman, Sten Sootla, Stephane Collot, Suchin Gururangan, Sydney Borodinsky, Tamar Herman, Tara Fowler, Tarek Sheasha, Thomas Georgiou, Thomas Scialom, Tobias Speckbacher, Todor Mihaylov, Tong Xiao, Ujjwal Karn, Vedanuj Goswami, Vibhor Gupta, Vignesh Ramanathan, Viktor Kerkez, Vincent Gonguet, Virginie Do, Vish Vogeti, Vitor Albiero, Vladan Petrovic, Weiwei Chu, Wenhan Xiong, Wenyin Fu, Whitney Meers, Xavier Martinet, Xiaodong Wang, Xiaofang Wang, Xiaoqing Ellen Tan, Xide Xia, Xinfeng Xie, Xuchao Jia, Xuewei Wang, Yaelle Goldschlag, Yashesh Gaur, Yasmine Babaei, Yi Wen, Yiwen Song, Yuchen Zhang, Yue Li, Yuning Mao, Zacharie Delpierre Coudert, Zheng Yan, Zhengxing Chen, Zoe Papakipos, Aaditya Singh, Aayushi Srivastava, Abha Jain, Adam Kelsey, Adam Shajnfeld, Adithya Gangidi, Adolfo Victoria, Ahuva Goldstand, Ajay Menon, Ajay Sharma, Alex Boesenberg, Alexei Baevski, Allie Feinstein, Amanda Kallet, Amit Sangani, Amos Teo, Anam Yunus, Andrei Lupu, Andres Alvarado, Andrew Caples, Andrew Gu, Andrew Ho, Andrew Poulton, Andrew Ryan, Ankit Ramchandani, Annie Dong, Annie Franco, Anuj Goyal, Aparajita Saraf, Arkabandhu Chowdhury, Ashley Gabriel, Ashwin Bharambe, Assaf Eisenman, Azadeh Yazdan, Beau James, Ben Maurer, Benjamin Leonhardi, Bernie Huang, Beth Loyd, Beto De Paola, Bhargavi Paranjape, Bing Liu, Bo Wu, Boyu Ni, Braden Hancock, Bram Wasti, Brandon Spence, Brani Stojkovic, Brian Gamido, Britt Montalvo, Carl Parker, Carly Burton, Catalina Mejia, Ce Liu, Changhan Wang, Changkyu Kim, Chao Zhou, Chester Hu, Ching-Hsiang Chu, Chris Cai, Chris Tindal, Christoph Feichtenhofer, Cynthia Gao, Damon Civin, Dana Beaty, Daniel Kreymer, Daniel Li, David Adkins, David Xu, Davide Testuggine, Delia David, Devi Parikh, Diana Liskovich, Didem Foss, Dingkang Wang, Duc Le, Dustin Holland, Edward Dowling, Eissa Jamil, Elaine Montgomery, Eleonora Presani, Emily Hahn, Emily Wood, Eric-Tuan Le, Erik Brinkman, Esteban Arcaute, Evan Dunbar, Evan Smothers, Fei Sun, Felix Kreuk, Feng Tian, Filippos Kokkinos, Firat Ozgenel, Francesco Caggioni, Frank Kanayet, Frank Seide, Gabriela Medina Florez, Gabriella Schwarz, Gada Badeer, Georgia Swee, Gil Halpern, Grant Herman, Grigory Sizov, Guanyi Zhang, Guna Lakshminarayanan, Hakan Inan, Hamid Shojanazeri, Han Zou, Hannah Wang, Hanwen Zha, Haroun Habeeb, Harrison Rudolph, Helen Suk, Henry Aspegren, Hunter Goldman, Hongyuan Zhan, Ibrahim Damlaj, Igor Molybog, Igor Tufanov, Ilias Leontiadis, Irina-Elena Veliche, Itai Gat, Jake Weissman, James Geboski, James Kohli, Janice Lam, Japhet Asher, Jean-Baptiste Gaya, Jeff Marcus, Jeff Tang, Jennifer Chan, Jenny Zhen, Jeremy Reizenstein, Jeremy Teboul, Jessica Zhong, Jian Jin, Jingyi Yang, Joe Cummings, Jon Carvill, Jon Shepard, Jonathan McPhie, Jonathan Torres, Josh Ginsburg, Junjie Wang, Kai Wu, Kam Hou U, Karan Saxena, Kartikay Khandelwal, Katayoun Zand, Kathy Matosich, Kaushik Veeraraghavan, Kelly Michelena, Keqian Li, Kiran Jagadeesh, Kun Huang, Kunal Chawla, Kyle Huang, Lailin Chen, Lakshya Garg, Lavender A, Leandro Silva, Lee Bell, Lei Zhang, Liangpeng Guo, Licheng Yu, Liron Moshkovich, Luca Wehrstedt, Madian Khabsa, Manav Avalani, Manish Bhatt, Martynas Mankus, Matan Hasson, Matthew Lennie, Matthias Reso, Maxim Groshev, Maxim Naumov, Maya Lathi, Meghan Keneally, Miao Liu, Michael L. Seltzer, Michal Valko, Michelle Restrepo, Mihir Patel, Mik Vyatskov, Mikayel Samvelyan, Mike Clark, Mike Macey, Mike Wang, Miquel Jubert Hermoso, Mo Metanat, Mohammad Rastegari, Munish Bansal, Nandhini Santhanam, Natascha Parks, Natasha White, Navyata Bawa, Nayan Singhal, Nick Egebo, Nicolas Usunier, Nikhil Mehta, Nikolay Pavlovich Laptev, Ning Dong, Norman Cheng, Oleg Chernoguz, Olivia Hart, Omkar Salpekar, Ozlem Kalinli, Parkin Kent, Parth Parekh, Paul Saab, Pavan Balaji, Pedro Rittner, Philip Bontrager, Pierre Roux, Piotr Dollar, Polina Zvyagina, Prashant Ratanchandani, Pritish Yuvraj, Qian Liang, Rachad Alao, Rachel Rodriguez, Rafi Ayub, Raghatham Murthy, Raghu Nayani, Rahul Mitra, Rangaprabhu Parthasarathy, Raymond Li, Rebekkah Hogan, Robin Battey, Rocky Wang, Russ Howes, Ruty Rinott, Sachin Mehta, Sachin Siby, Sai Jayesh Bondu, Samyak Datta, Sara Chugh, Sara Hunt, Sargun Dhillon, Sasha Sidorov, Satadru Pan, Saurabh Mahajan, Saurabh Verma, Seiji Yamamoto, Sharadh Ramaswamy, Shaun Lindsay, Shuang Feng, Shenghao Lin, Shengxin Cindy Zha, Shishir Patil, Shiva Shankar, Shuqiang Zhang, Shuqiang Zhang, Sinong Wang, Sneha Agarwal, Soji Sajuyigbe, Soumith Chintala, Stephanie Max, Stephen Chen, Steve Kehoe, Steve Satterfield, Sudarshan Govindaprasad, Sumit Gupta, Summer Deng, Sungmin Cho, Sunny Virk, Suraj Subramanian, Sy Choudhury, Sydney Goldman, Tal Remez, Tamar Glaser, Tamara Best, Thilo Koehler, Thomas Robinson, Tianhe Li, Tianjun Zhang, Tim Matthews, Timothy Chou, Tzook Shaked, Varun Vontimitta, Victoria Ajayi, Victoria Montanez, Vijai Mohan, Vinay Satish Kumar, Vishal Mangla, Vlad Ionescu, Vlad Poenaru, Vlad Tiberiu Mihailescu, Vladimir Ivanov, Wei Li, Wenchen Wang, Wenwen Jiang, Wes Bouaziz, Will Constable, Xiaocheng Tang, Xiaojian Wu, Xiaolan Wang, Xilun Wu, Xinbo Gao, Yaniv Kleinman, Yanjun Chen, Ye Hu, Ye Jia, Ye Qi, Yenda Li, Yilin Zhang, Ying Zhang, Yossi Adi, Youngjin Nam, Yu, Wang, Yu Zhao, Yuchen Hao, Yundi Qian, Yunlu Li, Yuzi He, Zach Rait, Zachary DeVito, Zef Rosnbrick, Zhaoduo Wen, Zhenyu Yang, Zhiwei Zhao, and Zhiyu Ma. The llama 3 herd of models, 2024. <https://arxiv.org/abs/2407.21783>.

Kaiming He, Xiangyu Zhang, Shaoqing Ren, and Jian Sun. Deep residual learning for image recognition, 2015. <https://arxiv.org/abs/1512.03385>.

Kaiming He, Haoqi Fan, Yuxin Wu, Saining Xie, and Ross Girshick. Momentum contrast for unsupervised visual representation learning. In *CVPR*, pages 9729–9738, 2020.

Kaiming He, Xin Chen, Saining Xie, Yanghao Li, and Piotr Dollár. Masked autoencoders are scalable vision learners. In *Proceedings of the IEEE/CVF Conference on Computer Vision and Pattern Recognition (CVPR)*, pages 16000–16009, 2022.

Olivier Hénaff, Aravind Srinivas, Jeffrey De Fauw, Ali Razavi, Carl Doersch, S. M. Ali Eslami, and Aäron van den Oord. Data-efficient image recognition with contrastive predictive coding. In *International Conference on Machine Learning (ICML)*, pages 4182–4192, 2020.

Yupeng Hou, Jiacheng Li, Ashley Shin, Jinsung Jeon, Abhishek Santhanam, Wei Shao, Kaveh Hassani, Ning Yao, and Julian McAuley. Generating long semantic ids in parallel for recommendation. In *Proceedings of the 31st ACM SIGKDD Conference on Knowledge Discovery and Data Mining V. 2*, pages 956–966, 2025.

J. Edward Hu, Yelong Shen, Phillip Wallis, Zeyuan Allen-Zhu, Yuanzhi Li, Shean Wang, and Weizhu Chen. Lora: Low-rank adaptation of large language models. *ArXiv*, abs/2106.09685, 2021. <https://api.semanticscholar.org/CorpusID:235458009>.

WeiQuan Huang, Aoqi Wu, Yifan Yang, Xufang Luo, Yuqing Yang, Liang Hu, Qi Dai, Xiyang Dai, Dongdong Chen, Chong Luo, and Lili Qiu. Llm2clip: Powerful language model unlocks richer visual representation. *ArXiv*, abs/2411.04997, 2024. <https://api.semanticscholar.org/CorpusID:273877534>.

Chao Jia, Yinfei Yang, Ye Xia, Yi-Ting Chen, Zarana Parekh, Hieu Pham, Quoc Le, Yun-Hsuan Sung, Zhen Li, and Tom Duerig. Scaling up visual and vision-language representation learning with noisy text supervision. In *International conference on machine learning*, pages 4904–4916. PMLR, 2021.

Will Kay, Joao Carreira, Karen Simonyan, Brian Zhang, Chloe Hillier, Sudheendra Vijayanarasimhan, Fabio Viola, Tim Green, Trevor Back, Paul Natsev, Mustafa Suleyman, and Andrew Zisserman. The kinetics human action video dataset, 2017. <https://arxiv.org/abs/1705.06950>.

Alexander Kirillov, Eric Mintun, Nikhila Ravi, Hanzi Mao, Chloe Rolland, Laura Gustafson, Tete Xiao, Spencer Whitehead, Alexander C Berg, Wan-Yen Lo, et al. Segment anything. In *Proceedings of the IEEE/CVF International Conference on Computer Vision*, pages 4015–4026, 2023.

Hilde Kuehne, Hueihan Jhuang, Estíbaliz Garrote, Tomaso A. Poggio, and Thomas Serre. Hmdb: A large video database for human motion recognition. *2011 International Conference on Computer Vision*, pages 2556–2563, 2011. <https://api.semanticscholar.org/CorpusID:206769852>.

Zhengfeng Lai, Vasileios Saveris, Chen Chen, Hong-You Chen, Haotian Zhang, Bowen Zhang, Juan Lao Tebar, Wenze Hu, Zhe Gan, Peter Grasch, et al. Revisit large-scale image-caption data in pre-training multimodal foundation models. In *ICLR*, 2025.

Doyup Lee, Chiheon Kim, Saehoon Kim, Minsu Cho, and Wook-Shin Han. Autoregressive image generation using residual quantization. In *Proceedings of the IEEE/CVF conference on computer vision and pattern recognition*, pages 11523–11532, 2022.

Yanghao Li, Haoqi Fan, Ronghang Hu, Christoph Feichtenhofer, and Kaiming He. Scaling language-image pre-training via masking. *2023 IEEE/CVF Conference on Computer Vision and Pattern Recognition (CVPR)*, pages 23390–23400, 2022. <https://api.semanticscholar.org/CorpusID:254125280>.

Youwei Liang, Chongjian Ge, Zhan Tong, Yibing Song, Jue Wang, and Pengtao Xie. Evit: Expediting vision transformers via token reorganizations. In *International Conference on Learning Representations*, 2022. <https://api.semanticscholar.org/CorpusID:251647803>.

Dhruv Mahajan, Ross Girshick, Vignesh Ramanathan, Kaiming He, Manohar Paluri, Yixuan Li, Ashwin Bharambe, and Laurens van der Maaten. Exploring the limits of weakly supervised pretraining, 2018. <https://arxiv.org/abs/1805.00932>.

Shlok Kumar Mishra, Joshua Robinson, Huiwen Chang, David Jacobs, Aaron Sarna, Aaron Maschinot, and Dilip Krishnan. A simple, efficient and scalable contrastive masked autoencoder for learning visual representations. *ArXiv*, abs/2210.16870, 2022. <https://api.semanticscholar.org/CorpusID:253237813>.

Norman Mu, Alexander Kirillov, David A. Wagner, and Saining Xie. Slip: Self-supervision meets language-image pre-training. *ArXiv*, abs/2112.12750, 2021. <https://api.semanticscholar.org/CorpusID:245424883>.

Muhammad Ferjad Naeem, Yongqin Xian, Xiaohua Zhai, Lukas Hoyer, Luc Van Gool, and Federico Tombari. Silc: Improving vision language pretraining with self-distillation. *arXiv preprint arXiv:2310.13355*, 2023.

Thao Nguyen, Samir Yitzhak Gadre, Gabriel Ilharco, Sewoong Oh, and Ludwig Schmidt. Improving multimodal datasets with image captioning. *Advances in neural information processing systems*, 36:22047–22069, 2023.

Maxime Oquab, Timothée Darcet, Théo Moutakanni, Huy Q. Vo, Marc Szafraniec, Vasil Khalidov, Pierre Fernandez, Daniel Haziza, Francisco Massa, Alaaeldin El-Nouby, Mahmoud Assran, Nicolas Ballas, Wojciech Galuba, Russ Howes, Po-Yao (Bernie) Huang, Shang-Wen Li, Ishan Misra, Michael G. Rabbat, Vasu Sharma, Gabriel Synnaeve, Huijiao Xu, Hervé Jégou, Julien Mairal, Patrick Labatut, Armand Joulin, and Piotr Bojanowski. Dinov2: Learning robust visual features without supervision. *ArXiv*, abs/2304.07193, 2023. <https://api.semanticscholar.org/CorpusID:258170077>.

Alec Radford, Jong Wook Kim, Chris Hallacy, Aditya Ramesh, Gabriel Goh, Sandhini Agarwal, Girish Sastry, Amanda Askell, Pamela Mishkin, Jack Clark, et al. Learning transferable visual models from natural language supervision. In *ICML*, 2021a.

Alec Radford, Jong Wook Kim, Chris Hallacy, Aditya Ramesh, Gabriel Goh, Sandhini Agarwal, Girish Sastry, Amanda Askell, Pamela Mishkin, Jack Clark, et al. Learning transferable visual models from natural language supervision. In *International Conference on Machine Learning*, pages 8748–8763. PMLR, 2021b.

Ali Razavi, Aaron Van den Oord, and Oriol Vinyals. Generating diverse high-fidelity images with vq-vae-2. *Advances in neural information processing systems*, 32, 2019.

Joshua Robinson, Ching-Yao Chuang, Suvrit Sra, and Stefanie Jegelka. Contrastive learning with hard negative samples. In *ICLR*, 2021.

Christoph Schuhmann, Romain Beaumont, Richard Vencu, Cade Gordon, Ross Wightman, Mehdi Cherti, Theo Coombes, Aarush Katta, Clayton Mullis, Mitchell Wortsman, Patrick Schramowski, Srivatsa Kundurthy, Katherine Crowson, Ludwig Schmidt, Robert Kaczmarczyk, and Jenia Jitsev. Laion-5b: An open large-scale dataset for training next generation image-text models. *ArXiv*, abs/2210.08402, 2022. <https://api.semanticscholar.org/CorpusID:252917726>.

Noam M. Shazeer and Mitchell Stern. Adafactor: Adaptive learning rates with sublinear memory cost. *ArXiv*, abs/1804.04235, 2018. <https://api.semanticscholar.org/CorpusID:4786918>.

Oriane Siméoni, Huy V. Vo, Maximilian Seitzer, Federico Baldassarre, Maxime Oquab, Cijo Jose, Vasil Khalidov, Marc Szafraniec, Seungeun Yi, Michaël Ramamonjisoa, Francisco Massa, Daniel Haziza, Luca Wehrstedt, Jianyuan Wang, Timothée Darcet, Théo Moutakanni, Leonel Santana, Claire Roberts, Andrea Vedaldi, Jamie Tolan, John Brandt, Camille Couprie, Julien Mairal, Hervé Jégou, Patrick Labatut, and Piotr Bojanowski. Dinov3, 2025. <https://arxiv.org/abs/2508.10104>.

Mannat Singh, Laura Gustafson, Aaron B. Adcock, Vinicius de Freitas Reis, Buğra Gedik, Raj Prateek Kosaraju, Dhruv Kumar Mahajan, Ross B. Girshick, Piotr Dollár, and Laurens van der Maaten. Revisiting weakly supervised pre-training of visual perception models. *2022 IEEE/CVF Conference on Computer Vision and Pattern Recognition (CVPR)*, pages 794–804, 2022. <https://api.semanticscholar.org/CorpusID:246063491>.

Mannat Singh, Quentin Duval, Kalyan Vasudev Alwala, Haoqi Fan, Vaibhav Aggarwal, Aaron Adcock, Armand Joulin, Piotr Dollár, Christoph Feichtenhofer, Ross Girshick, Rohit Girdhar, and Ishan Misra. The effectiveness of mae pre-pretraining for billion-scale pretraining. In *ICCV*, 2023.

Jianlin Su, Yu Lu, Shengfeng Pan, Bo Wen, and Yunfeng Liu. Roformer: Enhanced transformer with rotary position embedding. *ArXiv*, abs/2104.09864, 2021. <https://api.semanticscholar.org/CorpusID:233307138>.

Zeyi Sun, Ye Fang, Tong Wu, Pan Zhang, Yuhang Zang, Shu Kong, Yuanjun Xiong, Dahua Lin, and Jiaqi Wang. Alpha-clip: A clip model focusing on wherever you want. In *Proceedings of the IEEE/CVF Conference on Computer Vision and Pattern Recognition (CVPR)*, pages 13019–13029, June 2024.

Yixuan Tang and Yi Yang. Pooling and attention: What are effective designs for llm-based embedding models?, 2024. <https://arxiv.org/abs/2409.02727>.

Gemma Team, Thomas Mesnard, Cassidy Hardin, Robert Dadashi, Surya Bhupatiraju, Shreya Pathak, Laurent Sifre, Morgane Rivière, Mihir Sanjay Kale, Juliette Love, et al. Gemma: Open models based on gemini research and technology. *arXiv preprint arXiv:2403.08295*, 2024.

Yonglong Tian, Dilip Krishnan, and Phillip Isola. Contrastive multiview coding. In *ECCV*, pages 776–794, 2020.

Shengbang Tong, Ellis Brown, Penghao Wu, Sanghyun Woo, Manoj Middepogu, Sai Charitha Akula, Jihan Yang, Shusheng Yang, Adithya Iyer, Xichen Pan, et al. Cambrian-1: A fully open, vision-centric exploration of multimodal llms. In *NeurIPS*, 2024.

Hugo Touvron, Thibaut Lavril, Gautier Izacard, Xavier Martinet, Marie-Anne Lachaux, Timothée Lacroix, Baptiste Rozière, Naman Goyal, Eric Hambro, Faisal Azhar, Aurélien Rodriguez, Armand Joulin, Edouard Grave, and Guillaume Lample. Llama: Open and efficient foundation language models. *ArXiv*, abs/2302.13971, 2023a. <https://api.semanticscholar.org/CorpusID:257219404>.

Hugo Touvron, Thibaut Lavril, Gautier Izacard, Xavier Martinet, Marie-Anne Lachaux, Timothée Lacroix, Baptiste Rozière, Naman Goyal, Eric Hambro, Faisal Azhar, et al. Llama: Open and efficient foundation language models. *arXiv preprint arXiv:2302.13971*, 2023b.

Du Tran, Lubomir Bourdev, Rob Fergus, Lorenzo Torresani, and Manohar Paluri. Learning spatiotemporal features with 3d convolutional networks, 2015. <https://arxiv.org/abs/1412.0767>.

Michael Tschannen, Manoj Kumar, Andreas Steiner, Xiaohua Zhai, Neil Houlsby, and Lucas Beyer. Image captioners are scalable vision learners too. *Advances in Neural Information Processing Systems*, 36, 2024.

Michael Tschannen, Alexey Gritsenko, Xiao Wang, Muhammad Ferjad Naeem, Ibrahim Alabdulmohsin, Nikhil Parthasarathy, Talfan Evans, Lucas Beyer, Ye Xia, Basil Mustafa, et al. Siglip 2: Multilingual vision-language encoders with improved semantic understanding, localization, and dense features. *arXiv preprint arXiv:2502.14786*, 2025.

Aäron van den Oord, Yazhe Li, and Oriol Vinyals. Representation learning with contrastive predictive coding. *preprint arXiv:1807.03748*, 2018.

Bo Wan, Michael Tschannen, Yongqin Xian, Filip Pavetic, Ibrahim Alabdulmohsin, Xiao Wang, André Susano Pinto, Andreas Steiner, Lucas Beyer, and Xiaohua Zhai. Locca: Visual pretraining with location-aware captioners. *arXiv preprint arXiv:2403.19596*, 2024.

Haohan Wang, Songwei Ge, Zachary Lipton, and Eric P Xing. Learning robust global representations by penalizing local predictive power. In *Advances in Neural Information Processing Systems*, pages 10506–10518, 2019.

Zhenda Xie, Zheng Zhang, Yue Cao, Yutong Lin, Jianmin Bao, Zhuliang Yao, Qi Dai, and Han Hu. Simmim: A simple framework for masked image modeling. In *CVPR*, pages 9653–9663, 2022.

Hu Xu, Saining Xie, Xiaoqing Ellen Tan, Po-Yao Huang, Russell Howes, Vasu Sharma, Shang-Wen Li, Gargi Ghosh, Luke Zettlemoyer, and Christoph Feichtenhofer. Demystifying clip data. *arXiv preprint arXiv:2309.16671*, 2023.

Jun Xu, Tao Mei, Ting Yao, and Yong Rui. Msr-vtt: A large video description dataset for bridging video and language. *2016 IEEE Conference on Computer Vision and Pattern Recognition (CVPR)*, pages 5288–5296, 2016. <https://api.semanticscholar.org/CorpusID:206594535>.

Xiaohua Zhai, Basil Mustafa, Alexander Kolesnikov, and Lucas Beyer. Sigmoid loss for language image pre-training. *2023 IEEE/CVF International Conference on Computer Vision (ICCV)*, pages 11941–11952, 2023a. <https://api.semanticscholar.org/CorpusID:257767223>.

Xiaohua Zhai, Basil Mustafa, Alexander Kolesnikov, and Lucas Beyer. Sigmoid loss for language image pre-training. In *ICCV*, 2023b.

Jinguo Zhu, Weiyun Wang, Zhe Chen, Zhaoyang Liu, Shenglong Ye, Lixin Gu, Yuchen Duan, Hao Tian, Weijie Su, Jie Shao, Zhangwei Gao, Erfei Cui, Yue Cao, Yangzhou Liu, Haomin Wang, Weiye Xu, Hao Li, Jiahao Wang, Han Lv, Dengnian Chen, Songze Li, Yinan He, Tan Jiang, Jiapeng Luo, Yi Wang, Cong He, Botian Shi, Xingcheng Zhang, Wenqi Shao, Junjun He, Ying Xiong, Wenwen Qu, Peng Sun, Penglong Jiao, Lijun Wu, Kai Zhang, Hui Deng, Jiaye Ge, Kaiming Chen, Limin Wang, Min Dou, Lewei Lu, Xizhou Zhu, Tong Lu, Dahua Lin, Yu Qiao, Jifeng Dai, and Wenhui Wang. Internvl3: Exploring advanced training and test-time recipes for open-source multimodal models. *ArXiv*, abs/2504.10479, 2025. <https://api.semanticscholar.org/CorpusID:277780955>.

A Model Architecture (Detailed)

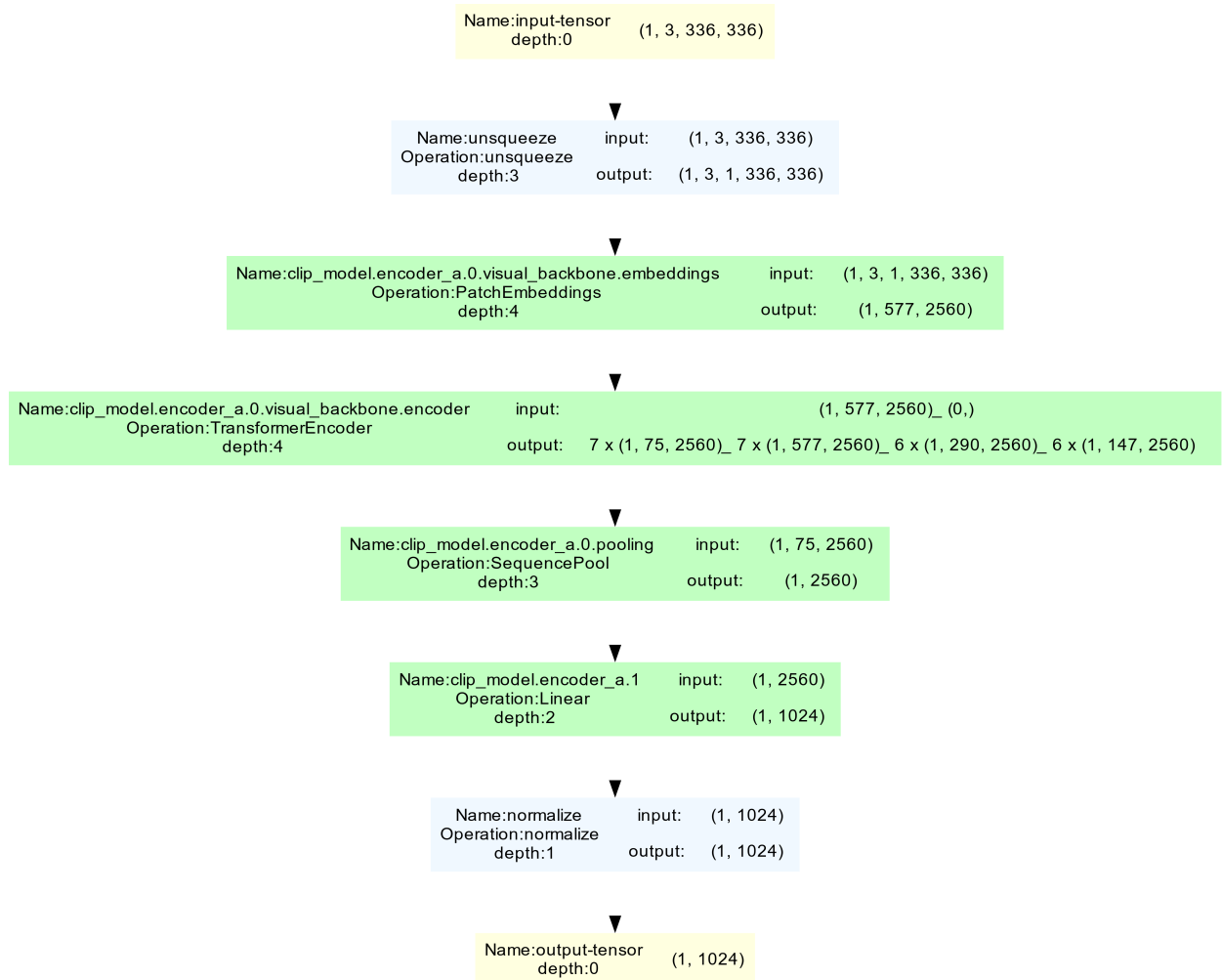


Figure 8 XrayVisual Model Overview